

# DESTIN: A new method for delineating the boundaries of crop fields by fusing spatial and temporal information from WorldView and Planet satellite imagery

Tao Cheng, Xusheng Ji, Gaoxiang Yang, Hengbiao Zheng, Jifeng Ma, Xia Yao, Yan Zhu, Weixing Cao\*

National Engineering and Technology Center for Information Agriculture (NETCIA), MARA Key Laboratory of Crop System Analysis and Decision Making, MOE Engineering Research Center of Smart Agriculture, Jiangsu Key Laboratory for Information Agriculture, Institute of Smart Agriculture, Nanjing Agricultural University, One Weigang, Nanjing, Jiangsu 210095, China



## ARTICLE INFO

### Keywords:

Field boundary delineation  
Imagery segmentation  
WorldView  
Planet  
Crop phenology

## ABSTRACT

The digital boundaries of crop fields represent a prerequisite for designing parcel-based crop management platforms, implementing online site-specific agronomic practices and monitoring crop growth per field. Previous approaches on field boundary delineation were mostly developed with medium resolution imagery (e.g., Landsat) for the regions or countries with intensive agriculture and large-sized crop fields. However, suitable delineation methods are scarce for the regions in developing countries where the majority of arable land is cultivated by smallholder farmers and distributed in small and fragmented crop fields. This study proposed a comprehensive method, delineation by fusing spatial and temporal information (DESTIN), to derive the boundaries of crop fields from sub-meter WorldView-2/3 and 3-m Planet imagery. After extraction of spatial objects from very high resolution (VHR) WorldView imagery, this method performed recognition of crop field objects using high resolution (HR) Planet-derived temporal features specifically concerning soil preparation and harvesting stages for summer crops. The performance of DESTIN in crop field boundary delineation was evaluated with the reference polygons (0.4–1.0 ha in area on average) over four subset areas in eastern China's Jiangsu province, and further compared with a benchmark objection extraction approach.

The results demonstrated that the integration of WorldView and Planet imagery as demanded by DESTIN yielded accurate recognition of crop fields with the classification overall accuracy (OA) ranging from 94.98% to 98.84%, which was remarkably improved over the use of WorldView or Planet imagery alone with increases in OA from 12% to 17%. The majority of crop field boundaries were successfully delineated with both methods, but DESTIN produced cleaner polygons than the benchmark approach and closer matches of field boundaries to the reference. DESTIN also yielded better one-to-one matches between delineations and reference (77% as opposed to 54%) and fewer one-to-many matches (1% as opposed to 33%) as a reflection of being less prone to oversegmentation. The DESTIN method does not need subjective parameterization for image segmentation, and could be applicable to the areas with availability of bi-temporal VHR imagery over the soil preparation and harvesting stages and HR imagery over the peak growth stage of summer crops. It has great potential for delineating the crop field boundaries in smallholder farming systems with VHR imagery acquired from satellite, airborne or unmanned aerial vehicle platforms.

## 1. Introduction

The demand for food security has been growing with the rapid increase of world population since the latter half of the 20th century, while the arable land has been experiencing tensions due to urbanization and land desertification, especially in the developing countries

represented by China (Tilman et al., 2001; Brown, 1995; FAO, 2009; Ministry of Natural Resources of the People's Republic of China, 2017). Furthermore, climate change in recent years has caused uncertainties in the increase of food production and unprecedented challenges for the balance between supply and demand. Accordingly, precision crop management has been increasingly adopted to produce more food with

\* Corresponding author.

E-mail address: [caow@njau.edu.cn](mailto:caow@njau.edu.cn) (W. Cao).

less input to the agricultural fields (Ata-Ul-Karim et al., 2013; Lemaire et al., 2008). In particular, the distribution and geometry of whole crop fields are highly desirable for designing parcel-based crop management measures (Abdul and Raju, 2009; Yang et al., 2017). With the advent of smart agriculture era, the digital boundary information of crop fields is even a prerequisite for farmland management information systems (Musat et al., 2018; Yu et al., 2017). The boundary of a crop field was defined as the location where a change in crop type occurs or a natural disruption could be seen between two similar crops (Rydberg and Borgefors, 2001). Conventionally, the digital boundary of a crop field is obtained by manually drawing its spatial extent in polygon (Basnyat et al., 2004), which is subjective, labour intensive, and time consuming. With increasingly available satellite imagery at various spatial resolutions, it becomes essential to develop image analysis methods for the accurate and efficient delineation of crop field boundaries.

Satellite imagery could be categorized into low, medium, high and very high spatial resolutions with the ground sampling distance (GSD) in the ranges of > 100 m, 10–100 m, 1–10 m and < 1 m, respectively (Aksoy et al., 2012; Jia et al., 2014). Moreover, crop fields could be divided into five levels in terms of area ( $A_{\text{field}}$ ): very large ( $A_{\text{field}} > 100 \text{ ha}$ ); large ( $16 \text{ ha} < A_{\text{field}} < 100 \text{ ha}$ ); medium ( $2.56 \text{ ha} < A_{\text{field}} < 16 \text{ ha}$ ); small ( $0.64 \text{ ha} < A_{\text{field}} < 2.56 \text{ ha}$ ); very small ( $A_{\text{field}} < 0.64 \text{ ha}$ ) (Lesiv et al., 2018). Many approaches have been developed for boundary delineation with medium resolution imagery from satellite instruments such as Landsat, Sentinel-2 and SPOT-4/5 (Graesser and Ramankutty, 2017; Ji, 1996; Rydberg and Borgefors, 2001; Turker and Kok, 2013; Watkins and Niekerk, 2019; Yan and Roy, 2014). Nevertheless, those approaches were mostly developed for the regions or countries with intensive agriculture and large-sized fields. Few of them were dedicated to the regions in developing countries represented by China, where small and fragmented crop fields dominate in the arable land and differ substantially in size from those in European and Americas (Fritz et al., 2015; Lesiv et al., 2018).

In the past two decades, the growing availability of sub-meter very high resolution (VHR) satellite imagery (e.g., WorldView and Pléiades) makes it possible to delineate the boundaries of crop fields, especially those with area < 2.56 ha. Although some studies have shown the necessity of multi-temporal high resolution (HR) imagery for accurate delineation of field boundaries (Alemu, 2016; Mueller et al., 2004), the acquisition of VHR imagery over multiple dates within a specific time frame remains a challenge for ordinary satellites (Jia et al., 2014; Zhang et al., 2013). Fortunately, multi-temporal HR satellite imagery becomes more accessible and affordable with the operational implementation of a new satellite system called Planet. It consists of 150–200 nano-satellites in orbit and is capable of acquiring 3–5 m multispectral imagery on a daily basis at low cost (Houborg and McCabe, 2016). Planet imagery has been used to detect crop sowing dates and estimate agronomic parameters, but not yet to delineate crop field boundaries (Li et al., 2019; Sadeh et al., 2019).

In general, the methods for delineating field boundaries from satellite imagery are categorized as 1) edge-based, 2) region-based and 3) hybrid that integrates the preceding two (Bhalerao and Wilson, 1990; Hossain and Chen, 2019; Turker and Kok, 2013; Wuest and Zhang, 2009). Edge-based methods use edge detectors such as Sobel, Scharr or Canny operators to extract crop field boundaries (Canny, 1986; Shrivakshan and Chandrasekar, 2012), which could be inaccurate in many cases since the edge detectors are susceptible to isolated objects and the extracted boundaries are not always obvious or closed (Mueller et al., 2004; Watkins and Niekerk, 2019). Region-based methods could overcome these disadvantages by extracting spatial objects according to regional homogeneity (Alemu, 2016; Mueller et al., 2004). Nevertheless, the resultant fields are often smaller in area than the truth because of the difference in growth status between the boundary and interior crops or the edge effect in crop cultivation (Chen et al., 2015). Hybrid methods are commonly used to integrate the advantages of

edge-based and region-based methods, and have shown superior performance over either type of method (Li et al., 2010; Moigne and Tilton, 2002; Rydberg and Borgefors, 2001). Moreover, their performance has been significantly improved with the use of multi-resolution segmentation algorithms (Aksoy et al., 2012; Chen et al., 2015; Debats et al., 2016), which are efficiently implemented in existing software packages such as eCognition Developer (Baatz and Schape, 2000). In addition to eCognition Developer, another commercial tool ENVI feature extraction or FX (ITT Visual Information Solutions, 2008) is also developed for automatically detecting and extracting objects edges from HR images (Poursanidis et al., 2015; Wang et al., 2015). It integrates the Sobel edge detection and multi-scale watershed segmentation algorithms invented by Jin (2012). In addition to spectral information, texture and spatial characteristics are also considered to delineate the object boundaries (Fetai et al., 2019). It is one of the most popular objection extraction tools and has been investigated for various applications (Poursanidis et al., 2015; Wang et al., 2015; Fetai et al., 2019). Nevertheless, the performance of boundary delineation for these algorithms is sensitive to the optimal segmentation parameters, which have to be setup by trial and error and often vary by location across the study area. These uncertainties make it difficult for these hybrid methods to be automated for efficient implementation over large areas.

In order to reduce human intervention and improve transferability, Yan and Roy (2014) proposed an automated method by integrating several algorithms and they further improved this method while extending the application from three states to the conterminous United States (Yan and Roy, 2016). The operation of these two variations could be automated but require sophisticated Landsat time series images and crop type classification as the input data, of which either type is scarce for the majority of regions in developing countries. Another Landsat-based automatic method developed by Graesser and Ramankutty (2017) does not need crop type classification data, but still needs *in situ* training samples for semi-supervised classification of major land cover types. Therefore, it is essential to develop an efficient method that could delineate the boundaries of crop fields automatically from satellite imagery and would not need additional crop type classification maps as the input. This may be feasible while using the temporal features derived from multi-temporal or time series images, which play an important role in cropland identification (Geerken, 2009; Qin et al., 2015). A few recent studies found that the knowledge-based features derived from cropland temporal trajectories of vegetation indices (VIs) could even be generalizable to multiple years in crop mapping without the need of *in situ* training data (Zhong et al., 2016; Xiong et al., 2017). In particular, these pertinent features on crop cycles include the stages of soil preparation or harvesting for the target crop (Waldner et al., 2015), which have great potential in help labeling the spatial objects accurately as crops and non-crop vegetation types.

In this study, we presented a comprehensive and hybrid method to delineate crop field boundaries from sub-meter WorldView and 3-m Planet imagery. This method was developed for the regions with heterogeneous agricultural landscape and smallholder farming systems. The research objectives were: 1) to develop a new method for automatically delineating the boundaries of crop fields from satellite multispectral imagery; 2) to examine the potential of integrating WorldView-based spatial information and Planet-based temporal information for identifying crop field objects; 3) to evaluate the proposed method over different sites in comparison with an object-based extraction method.

## 2. Study area and data

### 2.1. Study sites

Two sites were selected with one in Huai'an and the other in Xinghua, Jiangsu province of eastern China (Fig. 1) to represent variations in climate, crop field size and crop cultivation practice. The

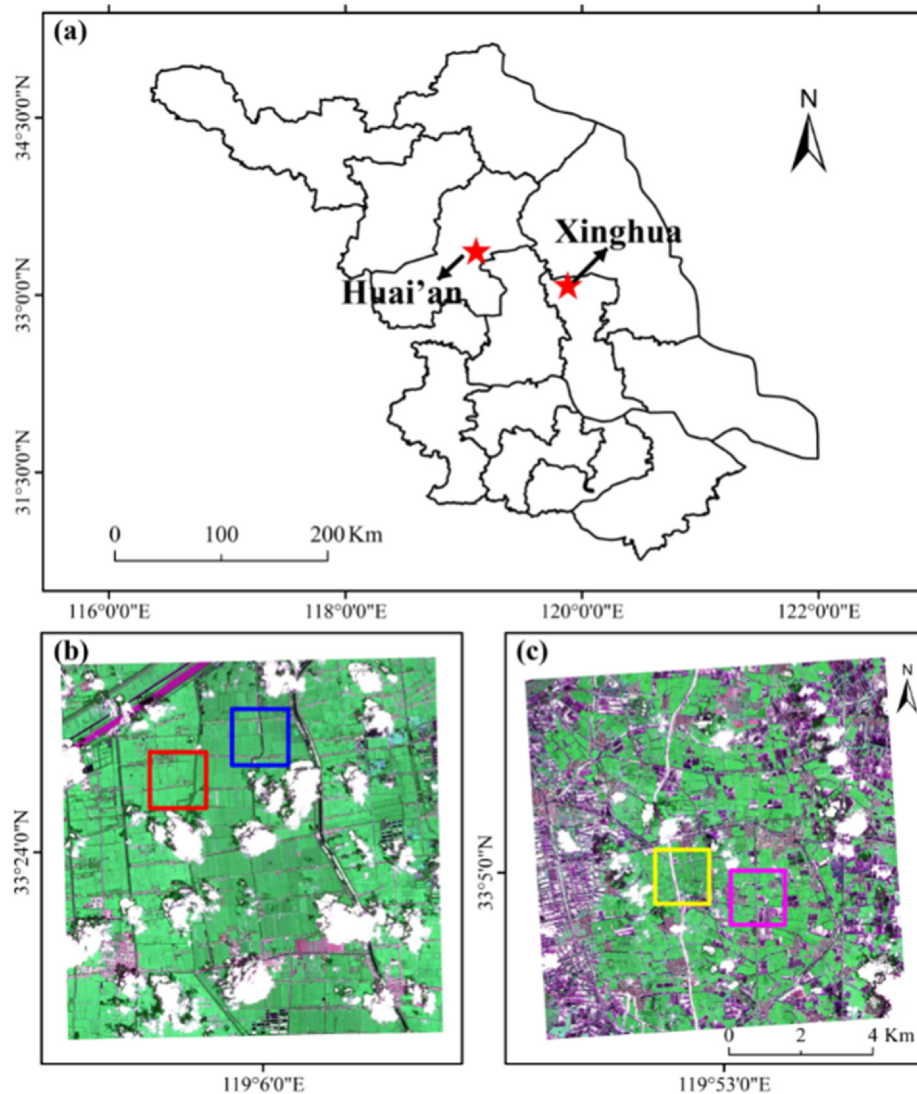


**Fig. 1.** (a) Location of the two study sites in Huai'an and Xinghua of Jiangsu province in eastern China and false color WorldView images covering (b) HA and (c) XH sites. The squares in red, blue, magenta, and yellow overlaid on the images represent the borders of subsets HA1, HA2, XH1, and XH2, respectively. All false color images are displayed with the combination of WorldView-2/3 red (R), near-infrared (G), and green (B) bands. (For interpretation of the references to color in this figure legend, the reader is referred to the web version of this article.)

Huai'an site (HA, 119°03'~119°09'E, 33°18'~33°27'N) from northern Jiangsu is located in the Yangtze-Huai Plain and is characterized by semi-humid monsoon climate with cold dry winters and warm humid summers. Rice and wheat rotation is the dominant cropping system in this area and crop fields are distributed in a mix of regular and irregular shapes. The Xinghua site (XH, 119°51'~119°54'E, 33°04'~33°06'N) from central Jiangsu belongs to the Lixia River Plain and is located in a subtropical humid monsoon climate zone with sufficient precipitation. Besides rice and wheat rotation, single-cropping pattern with rice cultivation has also become popular in recent years. The crop fields at the Huai'an site are generally smaller than those at the Xinghua site and mostly in irregular shapes.

In general, the crop fields with regular shapes were managed by state-owned farms or farmer cooperatives in intensive farming. These fields are often homogeneous in long strips as a result of uniform management practices by agricultural machinery. In contrast, the irregularly shaped crop fields are often managed by individual farmers in smallholder farming and could exhibit greater within-field variability due to diversity in agronomic practices. In addition, they may have narrow boundaries smaller than 0.5 m. Due to the difficulty in acquiring cloud-free sub-meter satellite imagery during the crop growing

season, we selected four subsets (HA1, HA2, XH1 and XH2) encompassing  $1.5 \times 1.5 \text{ km}^2$  ( $3000 \times 3000$  pixels) each within the study sites.

## 2.2. Crop calendar for the study sites

The crops grown at the study sites included rice and winter wheat in the majority, and maize, rapeseed, and soybean in the minority. They were categorized into winter crops and summer crops, with the former growing from late fall to early summer and the latter from mid-summer to mid-fall. From the harvesting period of winter crops to the sowing period of summer crops is the soil preparation stage when all crop fields are occupied by crop residues or bare soil (Fig. 2). However, non-crop vegetation types (e.g., evergreen forests, deciduous forests, and grasses) are under vigorous growth at this stage. This substantial offset of growth cycle is crucial for the discrimination between crops and non-crop vegetation and the identification of crop fields.

## 2.3. Satellite image data and preprocessing

Given the majority of small field sizes, high spatial resolution

|                 | Jan                                   | Feb | Mar | Apr | May | Jun                                   | Jul | Aug | Sep | Oct | Nov | Dec |
|-----------------|---------------------------------------|-----|-----|-----|-----|---------------------------------------|-----|-----|-----|-----|-----|-----|
|                 | Major growth periods for winter crops |     |     |     |     | Major growth periods for summer crops |     |     |     |     |     |     |
| Wheat           | Veg                                   | Sen | Har |     |     |                                       |     |     |     | Sow | Eme |     |
| Rapeseed        | Veg                                   | Sen | Har |     |     |                                       |     |     |     | Sow | Eme |     |
| Paddy rice      |                                       | Sow | Eme | Tra | Veg | Sen                                   | Har |     |     |     |     |     |
| Corn            |                                       | Sow | Eme | Veg | Sen | Har                                   |     |     |     |     |     |     |
| Soybean         |                                       | Sow | Eme | Veg | Sen | Har                                   |     |     |     |     |     |     |
| Grass           | Eme                                   | Veg |     |     |     |                                       | Sen |     |     |     |     |     |
| Deciduous Trees | Eme                                   | Veg |     |     |     |                                       | Sen |     |     |     |     |     |

**Fig. 2.** Growth cycles for the major vegetation types at the study sites. The blue boxes denote soil preparation stages before crop sowing or transplanting of summer crops. Note: Eme = Emergence stage (or green-up stage for deciduous trees), Har = Harvesting stage, Sen = Senescence stage, Sow = Sowing stage, Tra = Transplanting stage, Veg = Vegetative period. (For interpretation of the references to color in this figure legend, the reader is referred to the web version of this article.)

**Table 1**  
Specifications of the WorldView-2/3 and Planet images for boundary delineation.

| Imagery       | Spatial Resolution (m) | Band name | Wavelength (nm) |
|---------------|------------------------|-----------|-----------------|
| WorldView-2/3 | 0.5                    | Pan       | 450–1040        |
|               |                        | Coastal   | 400–450         |
|               | 2                      | Blue      | 450–510         |
|               |                        | Green     | 510–580         |
|               |                        | Yellow    | 585–625         |
|               |                        | Red       | 630–690         |
|               |                        | RE        | 705–745         |
|               |                        | NIR1      | 770–895         |
|               |                        | NIR2      | 860–1040        |
|               |                        | Blue      | 455–515         |
| Planet        | 3                      | Green     | 500–590         |
|               |                        | Red       | 590–670         |
|               |                        | NIR       | 780–860         |

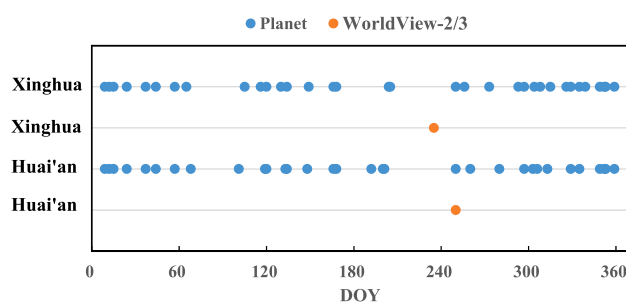


**Fig. 3.** Availability of the high spatial resolution satellite images and their temporal distribution over Huai'an and Xinghua sites.

WorldView and Planet satellite imagery was adopted to for delineation of field boundaries. The WorldView-2/3 satellite provides 0.5-m panchromatic and 2-m multispectral bands (Table 1). This study used two WorldView images, one taken on September 7th, 2015 over the Huai'an site (WorldView-2) and the other on 23rd August 2017 over the Xinghua site (WorldView-3) (Fig. 3). Raw WorldView-2/3 satellite images were converted to surface reflectance data through radiometric calibration and atmospheric correction in the software package ENVI 5.3 (Exelis Visual Information Solutions, Boulder, CO, USA). To facilitate boundary detection, the WorldView-2/3 multispectral reflectance

images were pan-sharpened to 0.5 m spatial resolution by the panchromatic bands with the Gram-Schmidt pan-sharpening method.

As the world's largest micro-satellite constellation, the Planet collects multispectral imagery in four bands at 3-m spatial resolution (Table 1). All cloud-free Planet surface reflectance products over the Huai'an and Xinghua sites from February 7, 2017 to March 1, 2018 were downloaded from the Planet Explorer (<https://www.planet.com>). This resulted in a total of 64 Planet images for a full rotation of rice and winter wheat, with 31 images for Huai'an and 34 for Xinghua. The 3-m Planet images were georeferenced to the WorldView-2/3 imagery and spatially resampled to the same spatial resolution (0.5 m) with the nearest neighbor approach for harmonization of multi-sensor data. Only the red and near-infrared (WorldView: 770–895 nm; Planet: 780–860 nm) bands needed for normalized difference vegetation index (NDVI) calculation were retained.

#### 2.4. Ground truth data

Ground surveys were carried out in 2017 to acquire boundaries of the crop fields covered by the four subset images. The geographical coordinates of crop field corners were collected through a RTK-GPS (Real-Time Kinematic Global Positioning System, CHC X900 GNSS) with the position error within 1 cm. The real-time dynamic accuracy of the RTK-GPS receiver in horizontal and vertical directions is  $\pm (10 + 1 \times 10^{-6} \times d)$  mm,  $\pm (20 + 1 \times 10^{-6} \times d)$  mm ( $d$  is the distance between the base and mobile stations), respectively. In addition, the position dilution of precision (PDOP) was smaller than 6 when the geographic coordinates were recorded. In addition, the information of land cover types and their distribution was recorded. Based on the geographical coordinates of field corners, the crop field boundaries were digitized manually through visual interpretation of WorldView-2/3 images. Here, digitization was only applied to the boundaries that could be visually interpreted on WorldView imagery (the boundaries were at least wider than 0.5 m). While the fields in intensive farming were generally uniform, each of the fields in smallholder farming exhibited obvious spatial variability and could be covered by crops with different growth stages, varieties, and agronomic practices (Fig. 4). Those spatial patterns within the smallholder managed fields did not necessarily mean the existence of natural boundaries visible on the WorldView imagery. The ground truth data encompassed the natural boundaries between individual crop fields, but not the sub-field spatial patterns. Boundaries narrower than 0.5 m might exist within the

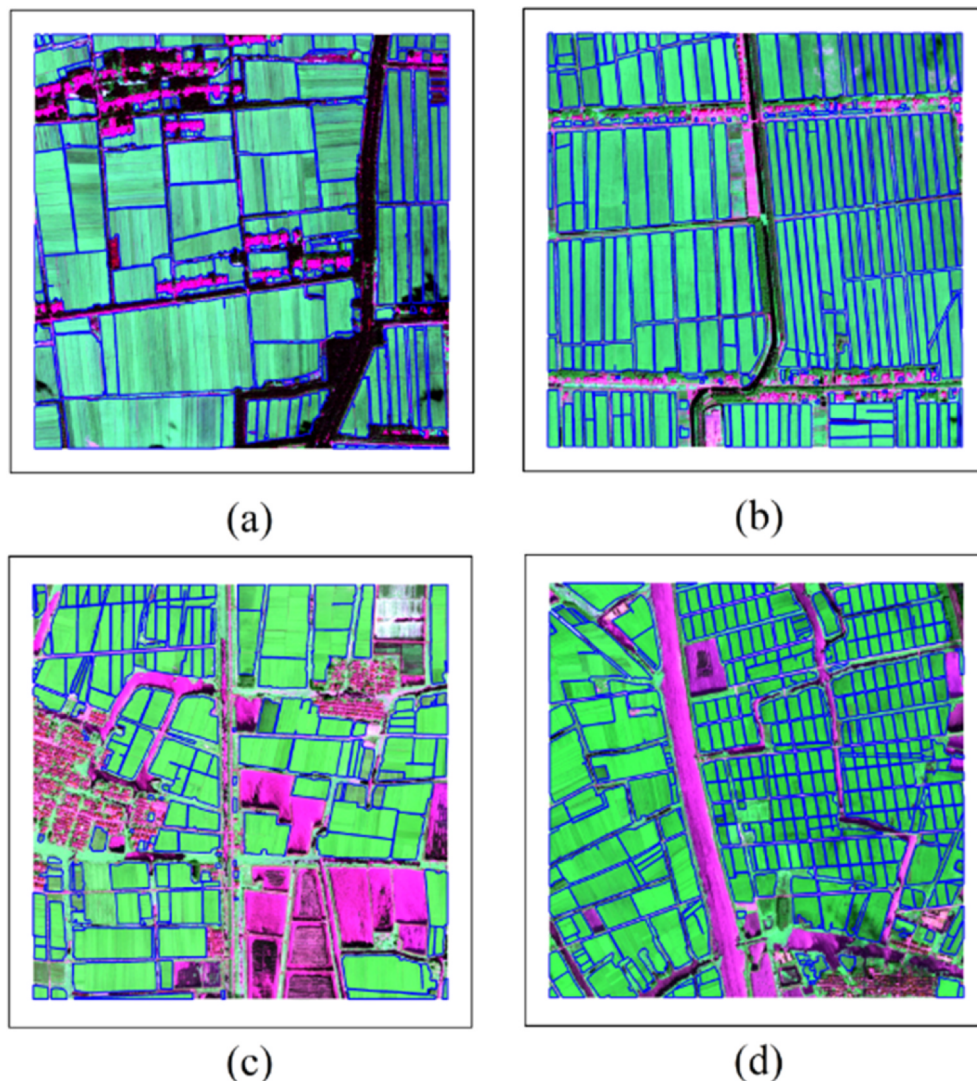


**Fig. 4.** Reference boundaries of the crop fields overlaid on the Worldview-2/3 false color images of the four subsets (a) HA1, (b) HA2, (c) XH1, and (d) XH2. The band combination of composite images is the same as that in Fig. 1b & c.

defined fields, but they were not considered for evaluating the automatic delineation method. This created a total of 961 crop fields as the reference boundary data.

### 3. Methodology

We proposed a new method, called DESTIN, for delineating the boundaries of crop fields by fusing spatial and temporal information from multi-sensor satellite imagery. This method used single-date WorldView-2/3 and multi-date Planet satellite images as the input and generated field crop boundaries as the output (Fig. 5). The comprehensive workflow mainly included four steps: 1) generation of edge intensity maps from WorldView images; 2) extraction of spatial objects from WorldView images; 3) identification of crop field objects from Planet images; and 4) refinement of crop field objects with morphological refinement. The details of each step are described in the following subsections.

#### 3.1. Generation of edge intensity maps

The edge intensity maps were generated from single-date WorldView-2/3 images with the technique developed by Yan and Roy (2014) for extracting crop fields from Landsat time series imagery

(Fig. 6). The edge intensity value of the center pixel in a  $3 \times 3$  convolution kernel was determined as the weighted sum of spectral distances between the center pixel and its neighboring pixels. Compared to individual bands, the use of multiple bands (e.g. NDVI) has been a common practice to produce great performance in land cover classification or crop field identification (Basnyat et al., 2004; Yan and Roy, 2014). In addition, the consistent use of NDVI images would help simplify the data processing chain of the DESTIN method. As a result, the spectral distances were determined in the NDVI derived from WorldView near-infrared and red reflectance bands instead of reflectance values as below:

$$\begin{aligned} D_k^{NDVI}(i, j) &= |NDVI(i, j) - NDVI(i + x(k), j + y(k))| \\ x(k = 1 \dots 8) &= \{0, -1, -1, -1, 0, 1, 1, 1\} \\ y(k = 1 \dots 8) &= \{1, 1, 0, -1, -1, -1, 0, 1\} \end{aligned} \quad (1)$$

where  $D_k^{NDVI}(i, j)$  is a measure of spectral distance in NDVI between the pixel location  $(i, j)$  and its 8-neighboring pixels.  $x(k = 1 \dots 8)$  and  $y(k = 1 \dots 8)$  are the locations of 8-neighboring pixels relative to the center pixel  $(i, j)$  in horizontal and vertical directions. The use of spectral distance measured in NDVI would enhance the separation of vegetation from non-vegetation pixels. Given the differences in relative location for the neighboring pixels, a weight coefficient ( $w$ ) was

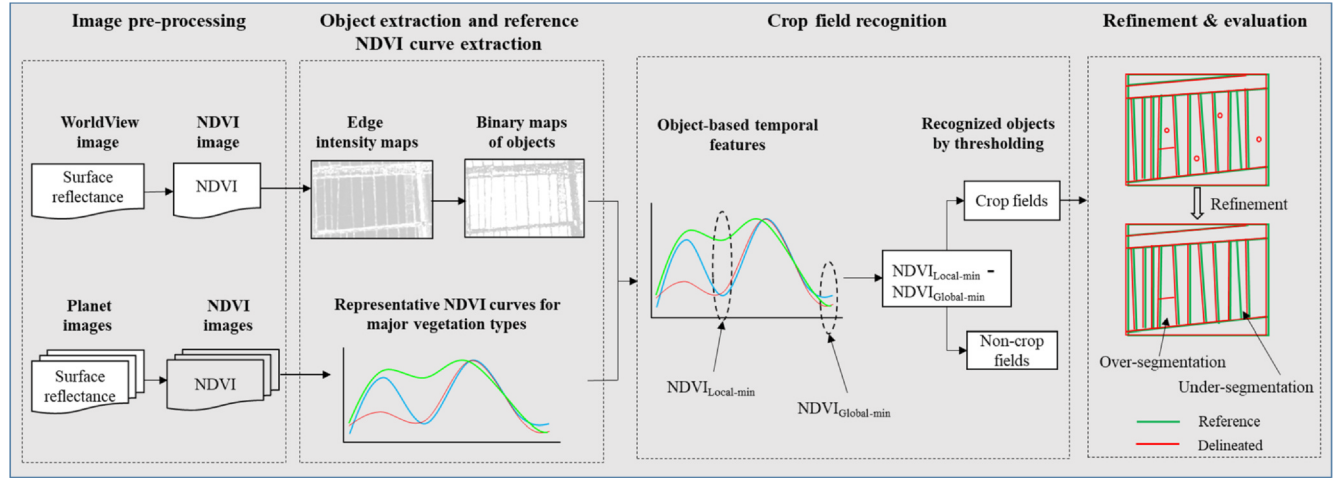


Fig. 5. Flowchart of the proposed DESTIN method for delineating crop field boundaries.

considered in the determination of spectral distances. The edge intensity value of a pixel  $e(i, j)$  was calculated as:

$$e(i, j) = \sum_{k=1}^8 D_k^{NDVI}(i, j) * w_k \quad (2)$$

$$w(k = 1 \dots 8) = \{1, \sqrt{2}/2, 1, \sqrt{2}/2, 1, \sqrt{2}/2, 1, \sqrt{2}/2\}$$

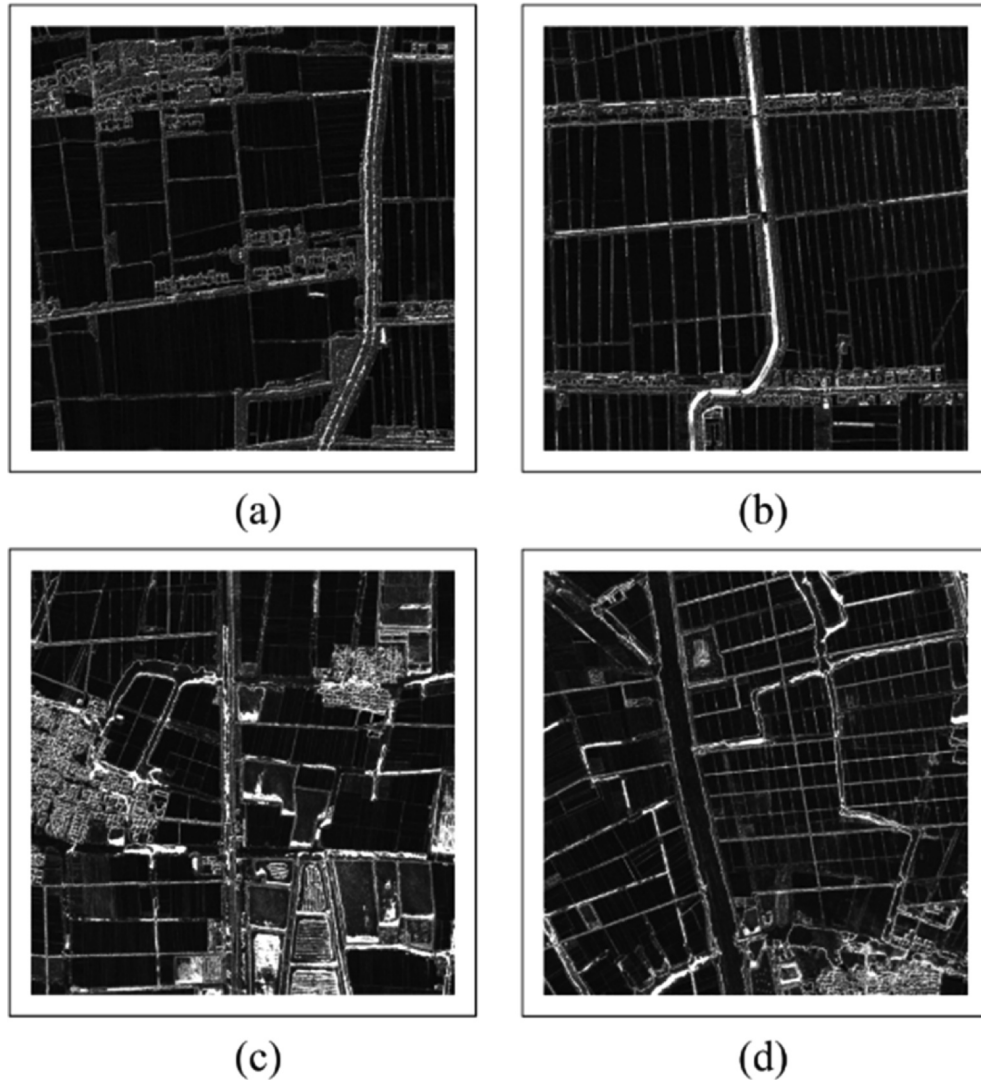
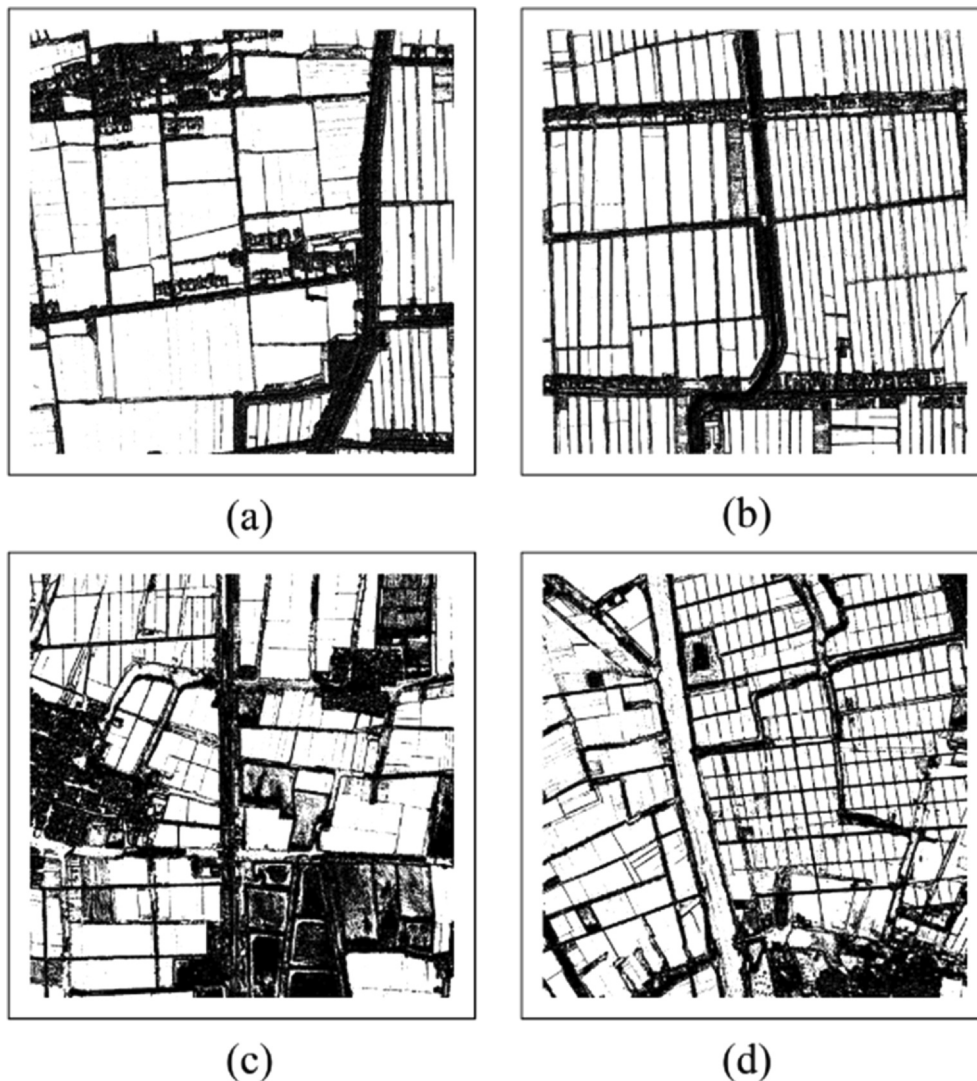


Fig. 6. The edge intensity maps derived from the WorldView imagery for the four subsets (a) HA1, (b), HA2, (c) XH1, and (d) XH2.



**Fig. 7.** Binary maps of spatial objects extracted from the edge intensity maps illustrated in Fig. 6.

where  $w(k = 1 \dots 8)$  are the weight coefficients determined by relative locations for the 8-neighboring pixels.  $w$  is equal to 1 for the neighboring pixels in horizontal and vertical directions and  $\sqrt{2}/2$  for diagonal neighbors of the  $3 \times 3$  convolution kernel.

### 3.2. Extraction of crop and non-crop objects

Image segmentation was applied to the edge intensity maps for extracting spatial objects. Before image segmentation, the multi-scale contrast limited adaptive histogram equalization (CLAHE) procedure was applied to adjust and standardize the local contrast of edge intensity values. Then, we used a multi-scale adaptive threshold segmentation (ATS) approach (Graesser and Ramankutty, 2017) to acquire binary spatial objects of crop fields and non-crop patches. A threshold was determined for each pixel from the surrounding local tile. ATS was exploited because a single threshold would not be applicable to the entire image due to the differences in illumination intensity, canopy coverage and crop growth status across regions. Therefore, we performed ATS to convert edge intensity values to binary values (edge or non-edge) (Fig. 7). The edge or no-edge value  $Edge(i, j)$  of each pixel was calculated as:

$$Edge(i, j) = \begin{cases} 1, & \text{if } e(i, j) < AdaptThresh(e(i, j)), \\ 0, & \text{otherwise} \end{cases} \quad (3)$$

where the thresholds  $AdaptThresh(e(i, j))_t$  were determined locally at scale  $t = 2000$ .

### 3.3. Recognition of crop field objects

The major land cover types at these study sites were grouped into crop (e.g., rice and soybean), non-crop vegetation (e.g., trees or grasses), and non-vegetation (e.g., water bodies or buildings) classes. The crop calendar information in Fig. 2 suggests that the existence of soil preparation stage in the crop rotation cycle would be beneficial to the spectral discrimination of crops from non-crop land cover types (Waldner et al., 2015). The overall trend in the NDVI time series curves exhibited the most distinctive pattern at the soil preparation stage among the three land cover types (Fig. 8). Although a sharp decline in NDVI was observed for the non-crop vegetation patch due to abnormal high temperature and drought in 2017, the NDVI value at soil preparation stage while adjusted for the overall trending would be substantially different from those of double-cropping and single-cropping fields. Since the time series data were only used for illustrating the significance of soil preparation and crop harvesting stages for land cover separation, temporal smoothing was not applied to the NDVI curves for simplicity purposes. At the soil preparation stage, the NDVI value reached a prominent local minimum ( $NDVI_{Local-min}$ ) for crops and the least prominent minimum for the non-crop vegetation (Table 2).

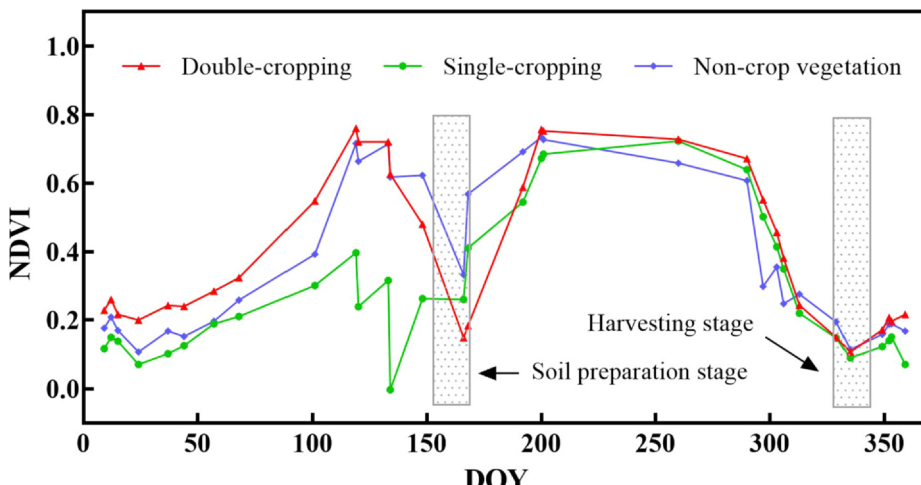


**Fig. 8.** The NDVI temporal curves extracted from time series Planet imagery over a double-cropping field, a single-cropping field and a non-crop vegetation patch in the HAI subset area. The grey areas overlaid on the temporal curves denote separately the soil preparation and crop harvesting stages for summer crops.

**Table 2**  
Temporal features and the corresponding interpretation.

| Feature                    | Crop cycle characteristics  |
|----------------------------|---|
| NDVI <sub>Spring-max</sub> | Peak growth stage of winter crops or non-crop vegetation in spring                      |
| NDVI <sub>Summer-max</sub> | Peak growth stage of summer crops in summer   |
| NDVI <sub>Local-min</sub>  | Bare soil or crop residue between harvesting of spring crops and sowing of summer crops |
| NDVI <sub>Global-min</sub> | No vegetation coverage or harvesting of summer crops                                    |

Considering the planting diversity within the study sites, the soil preparation stage was not consistent but dependent on crop type. To capture the spectral signature of this stage, we defined two critical points on the NDVI temporal curves, one for the local maximum NDVI in spring (NDVI<sub>Spring-max</sub>) and the other for the local maximum NDVI in summer (NDVI<sub>Summer-max</sub>) (Table 2). The soil preparation stage should fall between these two periods regardless of double-cropping fields, single-cropping fields and non-crop vegetation patches. To avoid comparing absolute NDVI values across regions, a reference point representing no vegetation coverage or the crop harvesting stage on the NDVI curves (NDVI<sub>Global-min</sub>) was adopted along with NDVI<sub>Local-min</sub> to characterize the NDVI changes for crop fields and non-crop vegetation patches. Empirical VI values are often used as thresholds for crop mapping with satellite imagery (Xiao et al., 2005). After trials with the NDVI values extracted from different land cover types as illustrated in Fig. 8, we found the values between 0.14 and 0.16 could be used as the threshold to distinguish spatial objects. Ultimately, we determined the minimum suitable NDVI value of 0.14 as the threshold of relative spectral difference. Although noises existed in the NDVI time series curves, the threshold was still suitable given the substantial differences in NDVI difference between crop fields and others. The rules derived from the temporal features NDVI<sub>Global-min</sub> and NDVI<sub>Local-min</sub> for identifying a crop field object were defined as:

$$\text{Object}(i) = \begin{cases} 1, & (\text{NDVI}_{\text{Local-min}} - \text{NDVI}_{\text{Global-min}} < 0.14) \\ 0, & (\text{NDVI}_{\text{Local-min}} - \text{NDVI}_{\text{Global-min}} \geq 0.14) \end{cases} \quad (4)$$

where Object(i) is the class value for a spatial object and *i* is the object number.

#### 3.4. Refinement with mathematical morphology operations

Morphological refinement (e.g., corrosion or expansion) is a widely used image processing procedure for cleaning spatial objects and has proved to be remarkable for improving the accuracy of spatial object

identification (Rishikeshan and Ramesh, 2018). After the identification of crop fields, we applied morphological opening and closing operations to further smooth the crop field boundaries and remove isolated small objects as the noise. Given the 0.5-m spatial resolution of pansharpened WorldView-2/3 images and the width of crop field boundaries (< 2.5 m), the size of filtering kernels used for these morphological operations were set as 5 × 5. Lastly, the raster-to-vector conversion was applied to all crop field objects to generate crop field boundaries.

#### 3.5. Accuracy assessment of boundary delineation

To evaluate the performance of DESTIN in delineating crop field boundaries, we conducted accuracy assessment in two aspects: identification of crop field objects and position of crop field boundaries.

##### 3.5.1. Recognition accuracy of crop field objects

The recognition for crop field objects was evaluated by the confusion matrix from object-based two-class classification. A total of 400 crop field objects and non-crop objects were selected per subset from the reference data for classification assessment. To evaluate the contribution of individual steps in the DESTIN method, we compared the classification accuracies in overall accuracy (OA) and kappa coefficient (Kappa) between four groups of procedures belonging to DESTIN. These included the field object recognitions with WorldView imagery alone, Planet imagery alone, the combination of WorldView and Planet imagery, and morphological refinement of the classification with combined satellite imagery. The first object recognition output was derived from the binary maps of spatial objects with WorldView imagery as defined in the first two steps of DESTIN. The second recognition output was performed by applying the threshold to the Planet-derived temporal features NDVI<sub>Global-min</sub> and NDVI<sub>Local-min</sub> following the third step alone. With the first three steps, the crop field objects were recognized as the third output by integrating WorldView and Planet imagery. This was followed by morphological cleaning as the fourth recognition output.

##### 3.5.2. Positional accuracy of crop field boundaries

In general, field boundaries delineated with image analysis approaches are assessed with four types of methods, naming visual inspection, system-level evaluation, goodness of fit and discrepancy measure (Li et al., 2011; Yang et al., 2015; Zhang et al., 2015). Although it is arbitrary and cannot provide quantitative evaluation, visual inspection is the most commonly used one due to its intuitiveness and simplicity (Zhang et al., 2008). The discrepancy measures can be used to quantitatively characterize the correspondence between an extracted object and the reference polygon by boundary match or spatial overlap,

so that the location errors of delineated crop field boundaries can be revealed (Zhang, 1996). In this study, we adopted visual inspection and discrepancy measure methods to evaluate the positional accuracy of delineated crop field boundaries. Empirical discrepancy was undertaken in local boundary location error and overall boundary location error. The local location errors of delineated boundaries were evaluated by the degree of under-segmentation ( $S_j^{under}$ ) and the degree of over-segmentation ( $S_j^{over}$ ), which indicate the degree the delineated crop field boundaries being larger and smaller than the reference, respectively. In addition, the overall location errors of delineated crop field boundaries were measured by a discrepancy measure of segmentation evaluation index (SEI), which is based on the two-sided 50% overlap of the corresponding object and is a more effective measure of segmentation quality under the condition of object recognition than traditional ones based on the one-sided 50% overlap (Yang et al., 2015). The degrees of under-segmentation, over-segmentation, and SEI of a delineated crop field  $E_j$  were defined as:

$$S_j^{under} = \left( 1 - \frac{|E_j \cap R_j|}{|R_j|} \right) \times 100\% \quad (5)$$

$$S_j^{over} = \left( 1 - \frac{|E_j \cap R_j|}{|E_j|} \right) \times 100\% \quad (6)$$

$$SEI_j^{local} = \sqrt{\frac{\left( 1 - \frac{|E_j \cap R_j|}{|R_j|} \right)^2 + \left( 1 - \frac{|E_j \cap R_j|}{|E_j|} \right)^2}{2}} \quad (7)$$

where  $E_j$  and  $R_j$  refer to the areas occupied by the delineated crop field boundaries and the reference, respectively.  $E_j \cap R_j$  represents the overlapping area of  $E_j$  and  $R_j$ .  $S_j^{under}$  and  $S_j^{over}$  values should fall in the 0 ~ 100% range and  $SEI_j^{local}$  values in 0 ~ 1. A smaller value of  $S_j^{under}$ ,  $S_j^{over}$  or  $SEI_j^{local}$  suggests a better match between delineated boundaries and the reference. Ideally, delineated crop field boundaries are completely consistent with the reference, with the values of  $S_j^{under}$ ,  $S_j^{over}$  and  $SEI_j^{local}$  equal to 0.

### 3.6. Comparison with the existing boundary delineation method

To further evaluate the performance of the DENSTIN method, we adopted the object extraction approach built in the commercial tool ENVI (Version 5.3.1), commonly known as Feature Extraction or ENVI FX (ITT Visual Information Solutions, 2008), as the benchmark boundary delineation solution. ENVI FX was selected against eCognition Developer due to the lower cost and seamless integration of boundary extraction with remote sensing image preparation and analysis in ENVI. This integrative environment will facilitate the data processing procedures for field-based crop monitoring with remotely sensed imagery within just one software system. The ENVI FX module could not make use of the temporal features from multi-sensor imagery and was implemented with the direct use of 0.5-m WorldView-2/3 full bands. It will produce closed boundaries for reasonable comparison with DESTIN. We tested the ENVI FX module with the same subsets and compared the delineated boundaries by visual inspection and empirical discrepancy.

The segmentation parameters for ENVI FX were determined by the commonly used trial and error approach (Watkins and Niekerk, 2019), by which the individual parameters varied independently and the resulting segmentation output was evaluated efficiently against reference field boundaries by visual interpretation and quantitative assessment of the SEI parameter. In addition, previous research has found that the scale parameter (i.e., Scale Level) has a bigger impact on the boundary delineation than other parameters (e.g., Merge Level and Texture Kernel Size) (Yang et al., 2015; Zhang et al., 2015). In this study, a range of Scale Level and Merge Level values had been tested for different subset images (Fig. 9). Eventually, we decided the appropriate

parameter combination by visually inspection of the segmentation outputs and quantitative comparison of the SEI values for different parameter combinations. As shown in Fig. 9, the segmentation quality became slightly better with the increase of Scale Level up to 60 and then deteriorated suddenly. The worst performance for a Scale Level of 80 in Fig. 9a & c was coincident with the disappearance of major boundaries in Fig. 9b & d. The segmentation quality did not change significantly for Merge Level ranging from 0 to 90 when Scale Level varied from 0 to 60. With this parameter assessment strategy, the final optimal segmentation parameters were determined separately for the HA and XH subsets (Table 3) based on the grid search on various parameter combinations.

## 4. Results

### 4.1. Recognition of crop field objects

**Table 4** displays the classification accuracy of crop and non-crop objects for the four recognition tasks. When performing edge detection and object extraction procedures, the accuracies for Huai'an subsets (HA1: OA = 84.88%; HA2: OA = 85.53%) were higher than those for Xinghua subsets (XH1: OA = 81.26%; XH2: OA = 79.76%). When only performing the crop object recognition procedure, the accuracies for Huai'an (HA1: OA = 80.05%; HA2: OA = 81.76) decreased by approximately 4% but those for Xinghua (XH1: OA = 82.85%; XH2: OA = 79.70%) did not change significantly. However, all those accuracies were markedly improved with overall accuracies exceeding 90% while adopting edge detection, object extraction and object recognition procedures. A further significant improvement in classification accuracy was even obtained for each of the subsets after applying morphological post-processing procedures, with a maximum increase by approximately 7% in OA.

### 4.2. Visual assessment of delineated crop field boundaries

**Fig. 10** shows the details of all spatial objects extracted with different classification approaches over a representative subset HA1. Crop field objects could be seen in the mono-temporal WorldView images but they appeared along with non-crop vegetation objects such as trees (Fig. 10a). The spatial details of individual crop fields could not be accurately retrieved in the Planet images, but the separation of crop objects from non-crop objects was more obvious. Only the road-side boundaries of crop fields, but not the boundaries between crop fields, could be identified (Fig. 10b). By integrating the complementary identification abilities from the WorldView and Planet imagery, the major non-crop objects were removed and the candidate objects of crop fields decreased substantially. Meanwhile, the boundaries of crop fields from WorldView imagery remained (Fig. 10c). With the morphological refinement, all the small noisy objects were filtered out and the boundaries of individual crop fields were clearly delineated (Fig. 10d).

**Figs. 11 and 12** represent the visual assessment of final crop field boundaries delineated with DESTIN in comparison with that using ENVI FX over the four subsets. Although the majority of crop field boundaries had been successfully delineated with both methods, the boundaries with DESTIN appeared much cleaner and closer to the truth than those with ENVI FX. Overall, DESTIN worked well for all these subsets and exhibited better performance than ENVI FX. In particular, false within-field boundaries could still be found in the output with ENVI FX for subsets HA1 and HA2 (Fig. 11c, d, g, & h). For subsets XH1 and XH2, the field boundaries were mixed up with many holes appearing within individual fields across different parts of the images (Fig. 12c, d, g, & h).

### 4.3. Area-based assessment of delineated crop field boundaries

The numbers of crop fields extracted with DESTIN and ENVI FX methods are 961 and 969, respectively. **Table 5** summarizes the

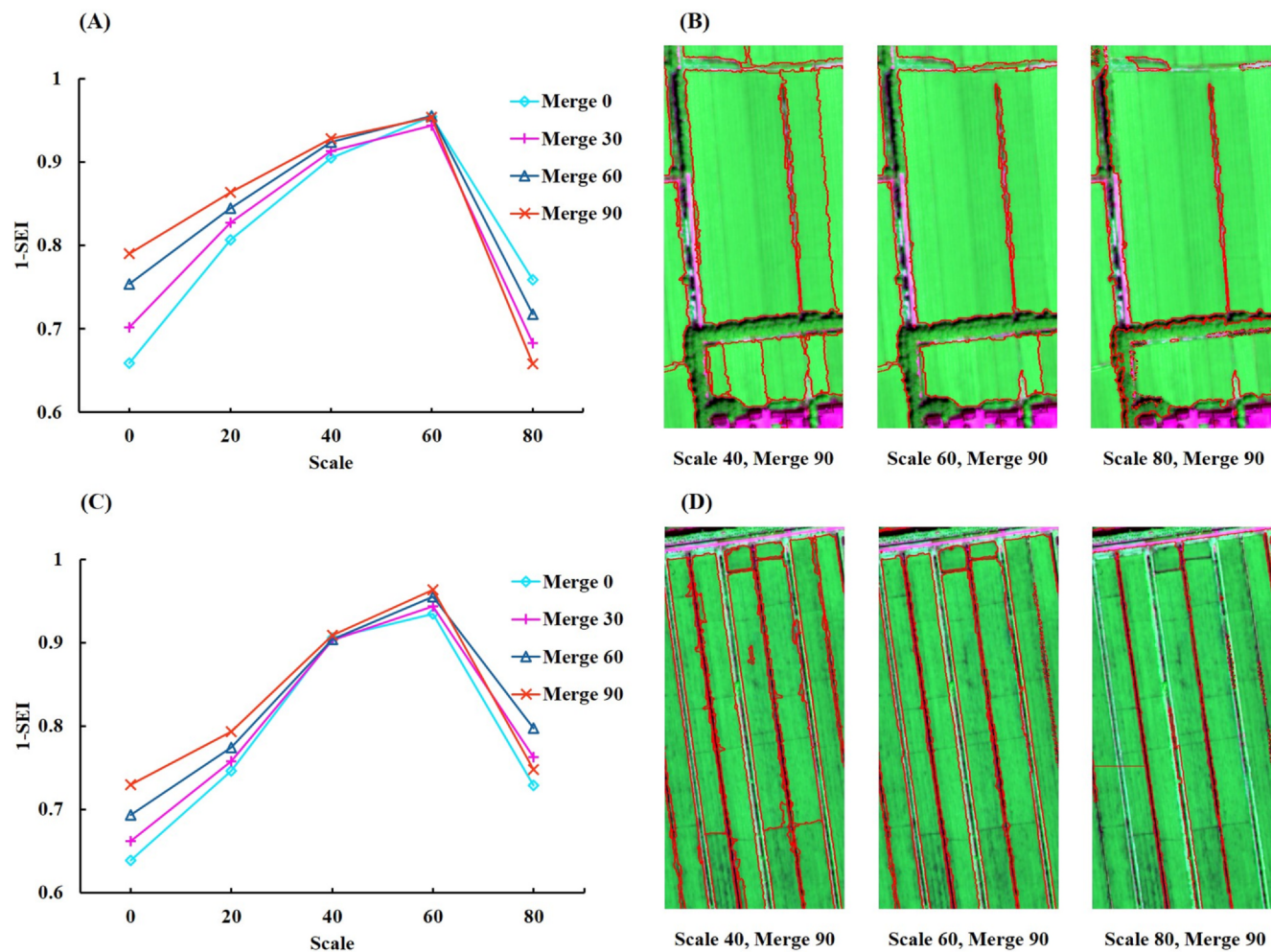


**Fig. 9.** Quantitative (a & c) and visual (b & d) assessment of segmentation quality over various combinations of segmentation parameters (Scale Level and Merge Level in ENVI FX) for two subset images with different field shapes.

**Table 3**  
Setup of segmentation parameters in ENVI FX for delineating crop field boundaries over the four subsets.

| Segmentation parameter | HA subsets | XH subsets |
|------------------------|------------|------------|
| Scale Level            | 60         | 60         |
| Merge Level            | 80         | 70         |
| Texture Kernel Size    | 3          | 3          |

proportions of correct matches between field objects delineated with DESTIN or ENVI FX and the reference. Compared to ENVI FX, DESTIN yielded a higher percentage of one-to-one matches (77% as opposed to 54%). The boundaries from ENVI FX (33%) exhibited a much higher number of one-to-many matches than those from DESTIN (1%), which is a reflection of excessive holes within the individual crop fields.

**Table 4**  
Classification accuracies for recognizing crop and non-crop objects over the four subsets with different groups of DESTIN procedures.

| Subset | Edge detection and object extraction with WorldView imagery |       | Recognition of crop field objects with Planet imagery |       | DESTIN without morphological cleaning with WorldView and Planet imagery |       | DESTIN with WorldView and Planet imagery |       |
|--------|---|-------|---|-------|---|-------|--|-------|
|        | OA (%)  | Kappa | OA (%)  | Kappa | OA (%)  | Kappa | OA (%)                                   | Kappa |
| HA1    | 84.88   | 0.70  | 80.05   | 0.60  | 91.99   | 0.84  | 98.84                                    | 0.98  |
| HA2    | 85.53   | 0.71  | 81.76   | 0.64  | 91.77   | 0.84  | 98.03                                    | 0.96  |
| XH1    | 81.26   | 0.61  | 82.45   | 0.63  | 90.02   | 0.80  | 94.98                                    | 0.90  |
| XH2    | 79.76   | 0.60  | 79.70   | 0.60  | 91.01   | 0.82  | 97.28                                    | 0.95  |

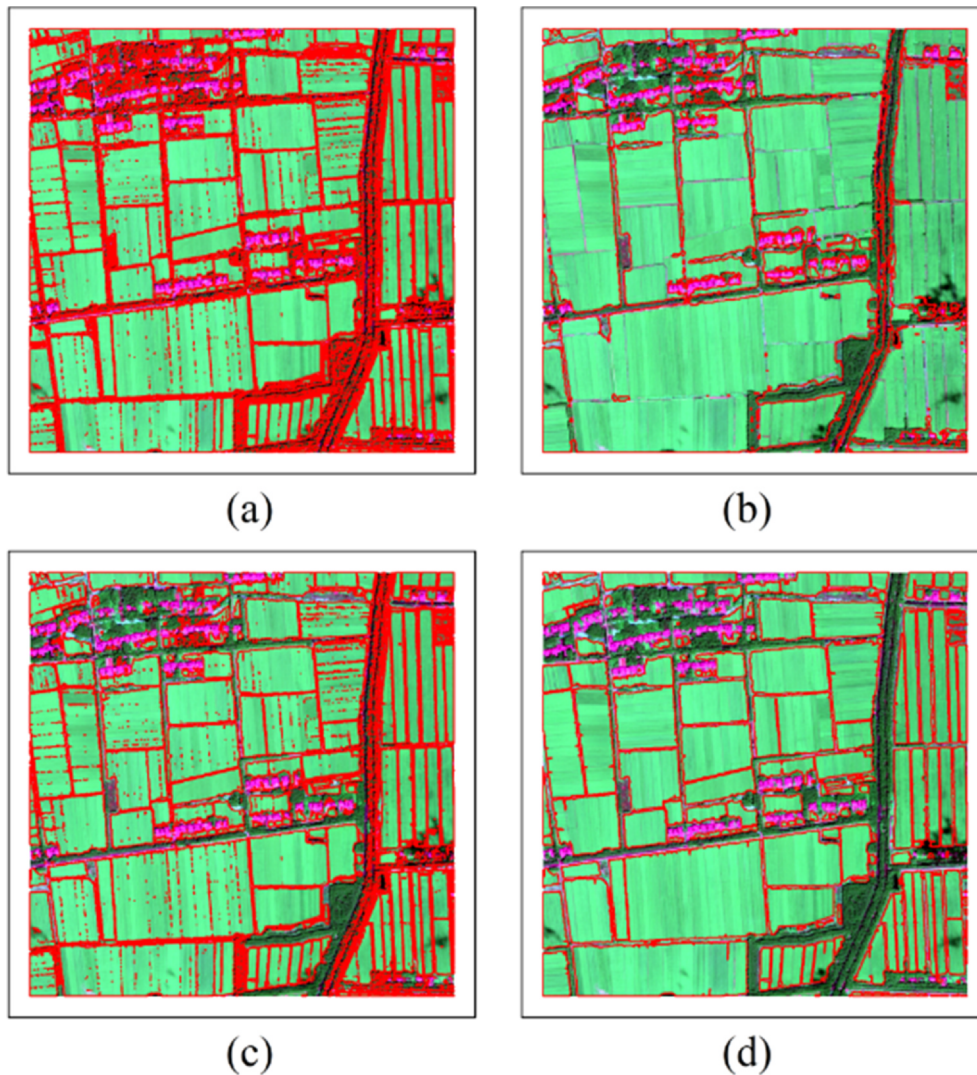


**Fig. 10.** Spatial objects extracted from (a) WorldView imagery, (b) Planet, (c) a combination of WorldView and Planet imagery, and (d) combined image data with morphological post-processing for the HA1 subset. The base image overlaid by these objects is a false color WorldView-2 composite (R: Red, G: NIR, B: Green) acquired on HA1 subset. (For interpretation of the references to color in this figure legend, the reader is referred to the web version of this article.)

were markedly higher than those for ENVI FX. For metrics < 20% or 0.2000, this trend remained consistent only for  $S^{over}$ .

## 5. Discussion

### 5.1. The importance of spatial details and crop calendar features in DESTIN

This study demonstrated that DESTIN achieved good performance in the delineation of crop fields, with spatial details from WorldView imagery and temporal details from Planet imagery. Due to the difference in spatial and temporal resolutions, WorldView and Planet imagery had played different roles in the delineation of crop field boundaries. From the WorldView imagery, DESTIN could delineate not only the major boundaries between spatial objects of different land cover types (e.g., crop fields and roads), but also the minor boundaries between spatial objects of the same land cover type (e.g., neighboring crop fields separated by narrower roads) (Fig. 10a). The use of WorldView imagery in delineating boundaries was also seen in a study by Mostafa (2020). In addition, these spatial details also contributed to the separation between crop and non-crop objects. However, some spatial objects in tree or other vegetation classes were mixed with crop fields due to the spectral similarity within only one WorldView image. Actually, previous research has suggested that it is often impossible to

discriminate between certain vegetation classes using only the spectral information in HR images (Aksøy et al., 2012; Helmholtz et al., 2014).

With multi-temporal Planet imagery, DESTIN could be used to pick out non-crop vegetation objects because they have different phenology or temporal variation from cultivated crops (Zhong et al., 2014). Non-crop and crop objects might exhibit similar spectral properties within a certain period, but that similarity would rarely remain stable in the entire growing season of crops. Therefore, crop field objects were recognized using the temporal information from Planet imagery (Fig. 10b). Relevant studies have reported the potential of crop calendar information in the delineation of crop field boundaries (Peña-Barragán et al., 2011; Xiong et al., 2017; Graesser and Ramankutty, 2017). Unlike those studies, the mere use of Planet imagery was insufficient for recognizing the narrow boundaries of the small crop fields in our study. Using the proposed DESTIN method, we integrated the spatial details and temporal features to improve the performance of crop field boundary delineation. The recognition accuracy of crop field objects from the combined data was remarkably improved compared to that from either type of information (Table 4), which was consistent with previous studies on crop classification (Sun et al., 2019; Jia et al., 2014).

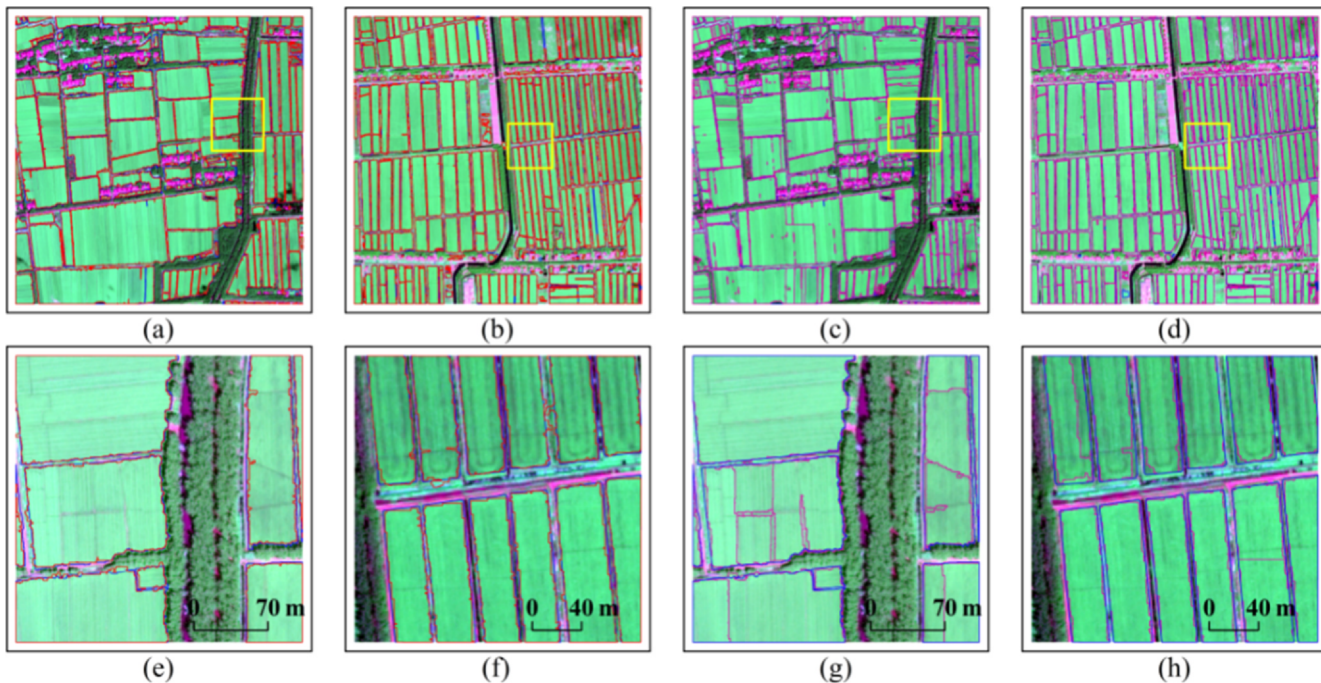


**Fig. 11.** The crop field boundaries delineated using (a, b) DESTIN (red lines) and (c, d) ENVI FX (magenta lines) overlaid on referenced field boundaries (blue lines) for subsets HA1 (a, c), HA2 (b, d). e-h represent the close-up views of the boundary details for the yellow squared area marked in a-d, respectively. (For interpretation of the references to color in this figure legend, the reader is referred to the web version of this article.)

## 5.2. The reliability of DESTIN

The core steps of DESTIN are extraction of spatial objects and recognition of crop field objects. While the performance of object extraction is closely related to the determination of edge intensity, the accuracy of crop field object recognition is attributed to the temporal features in the local crop calendar.

Due to the spectral similarity between crops and non-crop

vegetation, the discrimination by spectral difference alone is not always sufficient when they are at full leaf cover (Aksoy et al., 2012). Therefore, many algorithms (e.g., standard deviation, variance or coefficient of variation) were developed for enhancing crop field boundaries (North et al., 2019). In this study, we used edge intensity to highlight the contrast of adjacent spatial objects. Specifically, the edge intensity maps were derived from NDVI imagery to suppress the non-vegetation information (Yan and Roy, 2014). Some studies also used multi-

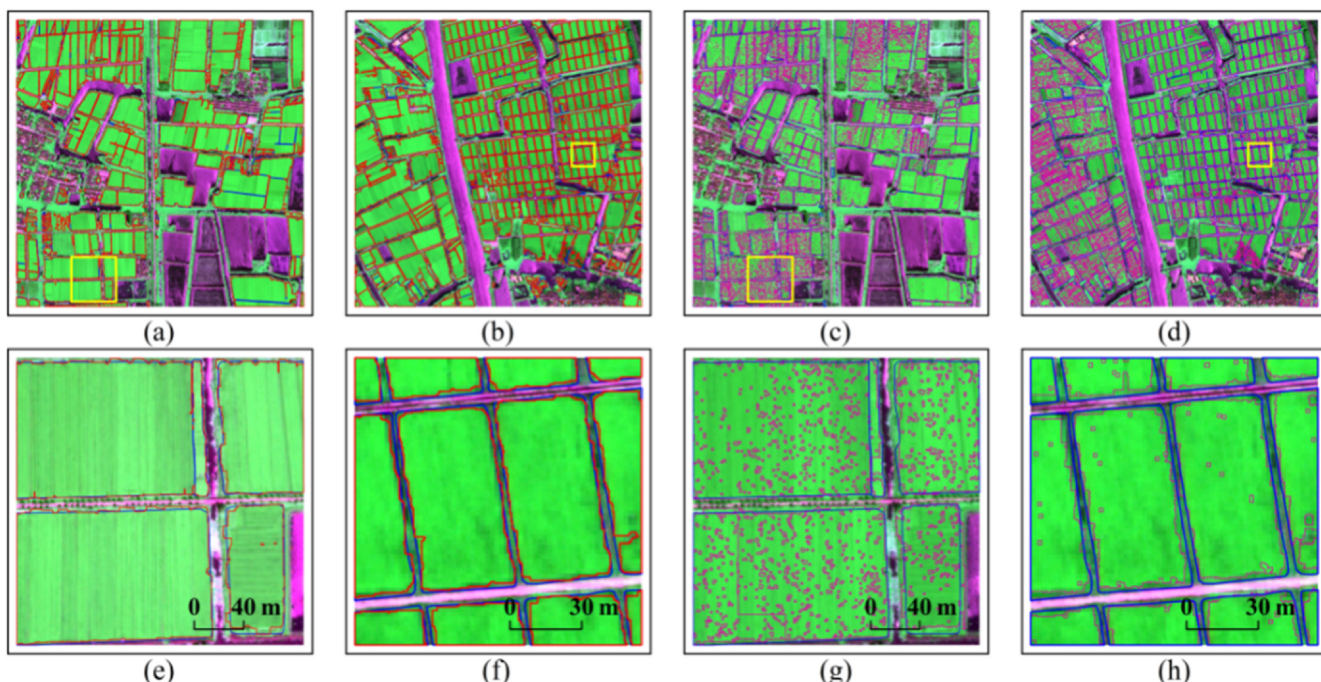


**Fig. 12.** The crop field boundaries delineated using (a, b) DESTIN (red lines) and (c, d) ENVI FX (magenta lines) overlaid on referenced field boundaries (blue lines) for subsets XH1 (a, c), XH2 (b, d). e-h represent the close-up views of the boundary details for the yellow squared area marked in a-d, respectively. (For interpretation of the references to color in this figure legend, the reader is referred to the web version of this article.)

**Table 5**

Correspondences of DESTIN or ENVI FX delineated crop field boundaries with the reference polygons for the four subsets.

| Type of matches between delineations and reference | Crop field boundaries delineated with DESTIN (961 units) | Crop field boundaries delineated with ENVI FX (969 units) |
|--|--|---|
| One-to-one   | 77% (743)  | 54% (523)   |
| One-to-many (over-segmented)                       | 1% (11)  | 33% (320)   |
| Many-to-one (under-segmented)                      | 11% (197)  | 8% (76)   |
| Many-to-many                                       | 1% (10)  | 5% (50)   |

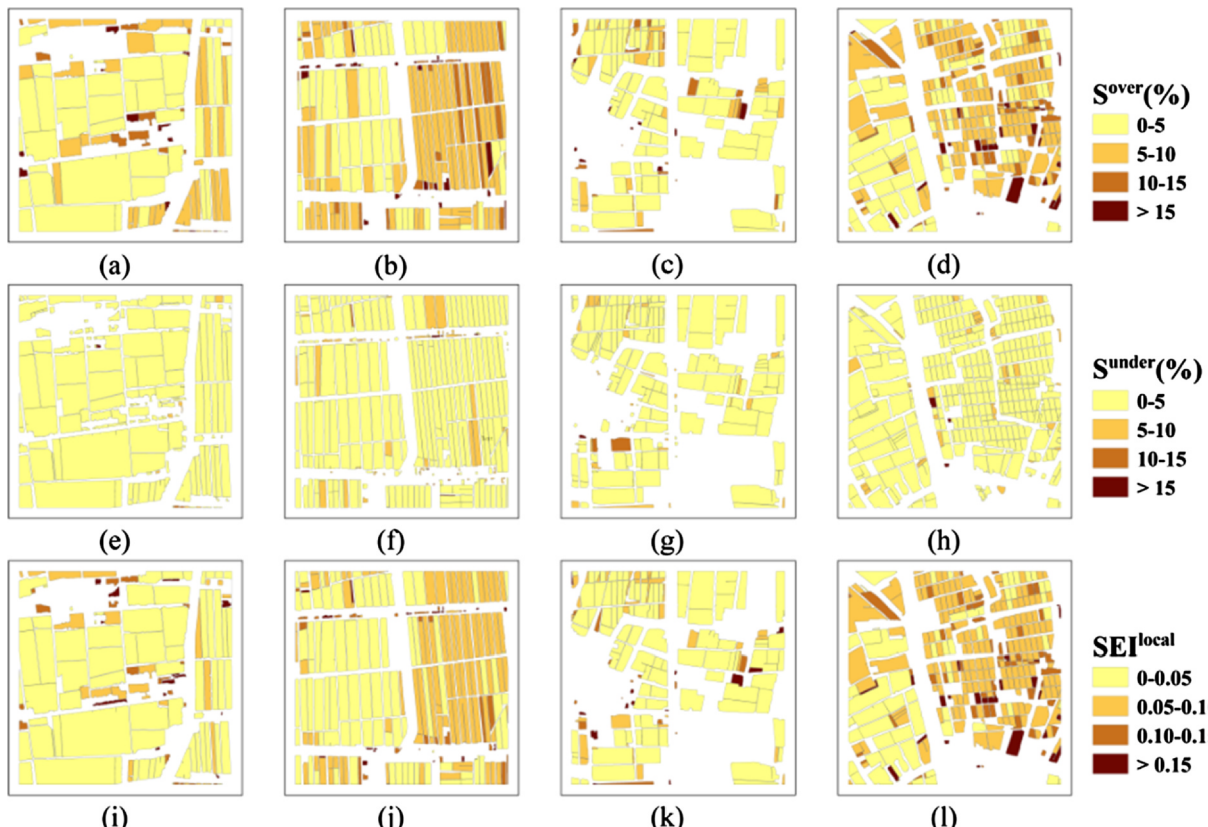


**Fig. 13.** Validation of the individual crop field boundaries through segmentation evaluation metrics  $S_{over}$ ,  $Sunder$  and  $SEI_{local}$  for the subsets HA1 (a, e, i), HA2 (b, f, j), XH1 (c, g, k), and XH2 (d, h, l).

temporal images to calculate the standard deviation for each band and then merge the multiple layers of statistical metrics into one composite with appropriate weighting (North et al., 2019). That way the determination of weights may increase human interference and enhance the computational complexity. These procedures were simplified for DESTIN by the use of an NDVI image directly derived from the multi-spectral imagery. Furthermore, the edge intensity maps were further standardized by histogram equalization to eliminate noise interference.

Based on the edge intensity maps, a segmentation operation (ATS) was adopted in the DESTIN method to extract spatial objects. The ATS operation has some advantages over the segmentation algorithms commonly used in field boundary delineation studies, including watershed segmentation and multi-resolution segmentation (Butenuth

et al., 2004; Li et al., 2010). Those segmentation algorithms have functional parameters to setup for a given image scene, which could induce instability and inappropriateness across the image because the parameters are susceptible to the analyst's experience and spectral changes at different locations (Conrad et al., 2010; Weissteiner et al., 2015). With the DESTIN method, the segmentation threshold in the ATS operation was determined per pixel automatically from the local tile window centering at each pixel to be processed (Graesser and Ramankutty, 2017). In addition, DESTIN is not prone to over-segmentation, which often occurs to watershed segmentation algorithms and results in a large number of isolated objects (Bleau and Leon, 2000; Gonzalez and Woods, 2008). This should probably explain the small isolated holes within the crop fields as seen in Fig. 12c & d with the

**Table 6**

Comparison of segmentation accuracy metrics in  $Sunder$ ,  $S_{over}$  and  $SEI_{local}$  for the crop field boundaries delineated with DESTIN and ENVI FX methods.

| Statistical metric                                 | DESTIN   |            |               | ENVI FX  |            |               |
|--|----------|------------|---------------|----------|------------|---------------|
|  | $Sunder$ | $S_{over}$ | $SEI_{local}$ | $Sunder$ | $S_{over}$ | $SEI_{local}$ |
| Mean   | 12.94%   | 3.24%      | 0.0972        | 19.33%   | 4.19%      | 0.1054        |
| Proportion of fields with metric < 10% (or 0.1000) | 61.71%   | 96.28%     | 69.25%        | 46.44%   | 87.93%     | 62.02%        |
| Proportion of fields with metric < 20% (or 0.2000) | 80.70%   | 98.76%     | 87.51%        | 82.77%   | 95.25%     | 89.00%        |

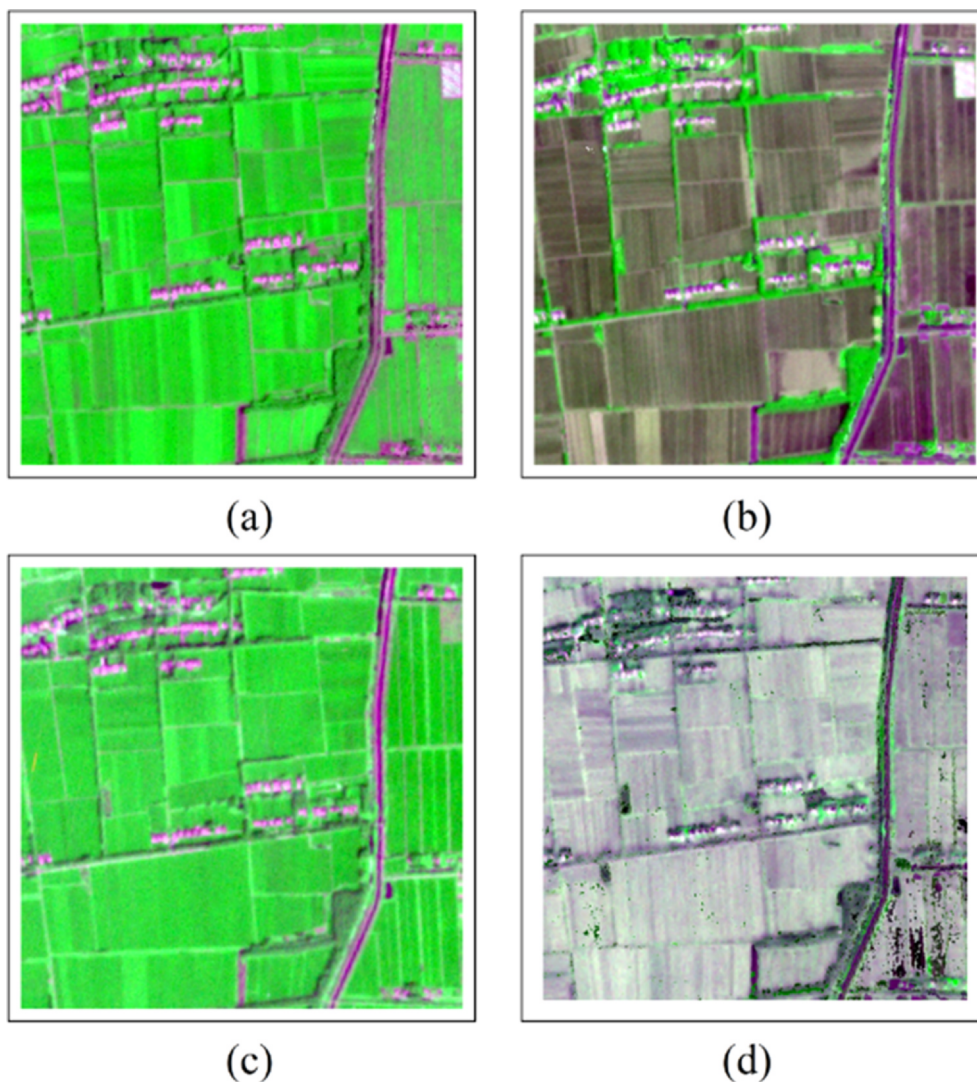


**Fig. 14.** False color composites of Planet satellite imagery over the subset HA1 for the dates corresponding to the occurrence of (a)  $\text{NDVI}_{\text{Spring-max}}$ , (b)  $\text{NDVI}_{\text{Local-min}}$ , (c)  $\text{NDVI}_{\text{Summer-max}}$ , and (d)  $\text{NDVI}_{\text{Global-min}}$ . The band combination of composite images is the same as that in Fig. 1b & c.

#### ENVI FX method.

The distinction between crop and non-crop objects in previous studies is mostly based on supervised or semi-supervised classification, which needs a certain number of defined samples to train the classifier (Graesser and Ramankutty, 2017; Watkins and Niekerk, 2019). In contrast, the recognition of crop field objects with DESTIN did not require training samples and only depended on the spectral signatures from soil preparation and crop harvesting stages. The crop fields were covered by bare soil at the stages of both soil preparation and crop harvesting (Fig. 14), but non-crop vegetation (e.g., grass and deciduous trees) in the study area exhibited continuous growth over this period and did not have a break in canopy coverage. In particular, we could see a drop over June in the NDVI curve for non-crop vegetation (Fig. 8). This decline in NDVI was not so significant as those for crops and was probably due to the change of vegetation coverage in response to the insufficient precipitation and high temperature (Figs. S1 & S2) (A et al., 2016). In a study by Waldner et al. (2015) they also indicated the possibility of separating crops and non-crop plants at soil preparation stage, but they did not investigate it explicitly for such a purpose.

Although the spectral difference between crops and non-crop plants was prominent at soil preparation stage (Fig. 8, Fig. 14b), it was not significant due to the senescence of all plants at the crop harvesting stage (Fig. 2). As a result, the crop and non-crop objects could be

distinguished by the difference between  $\text{NDVI}_{\text{Local-min}}$  derived from the soil preparation stage and  $\text{NDVI}_{\text{Global-min}}$  from the harvesting stage. This difference between crop and non-crop objects was so substantial that the NDVI difference threshold would not largely affect the performance of DESTIN. If the drop in NDVI at soil preparation stage were less significant for non-crop vegetation, the difference between  $\text{NDVI}_{\text{Local-min}}$  and  $\text{NDVI}_{\text{Global-min}}$  would be even greater and it would be easier to apply this threshold. Nevertheless, thresholds of various vegetation indices have been used for more than a decade in phenology-based algorithms for crop mapping due to the simplicity and interpretability of thresholding operations (Xiao et al., 2005; Dong et al., 2016). If one is concerned about the suitability of our threshold (0.14), they could adjust the threshold with the two Planet-derived NDVI images corresponding to soil preparation and summer crop harvesting stages.

#### 5.3. Advantages of DESTIN and implications for future application

Given the low revisit frequency and cloud coverage, it is challenging to acquire HR satellite imagery over the growing seasons of specific crops. This has hindered the development of crop field boundary delineation over large areas with small fields (Turker and Kok, 2013; Neigh et al., 2018) (Fig. 15). The fusion of multi-source satellite imagery is frequently used for accurate classification of crop types (Zhu et al.,

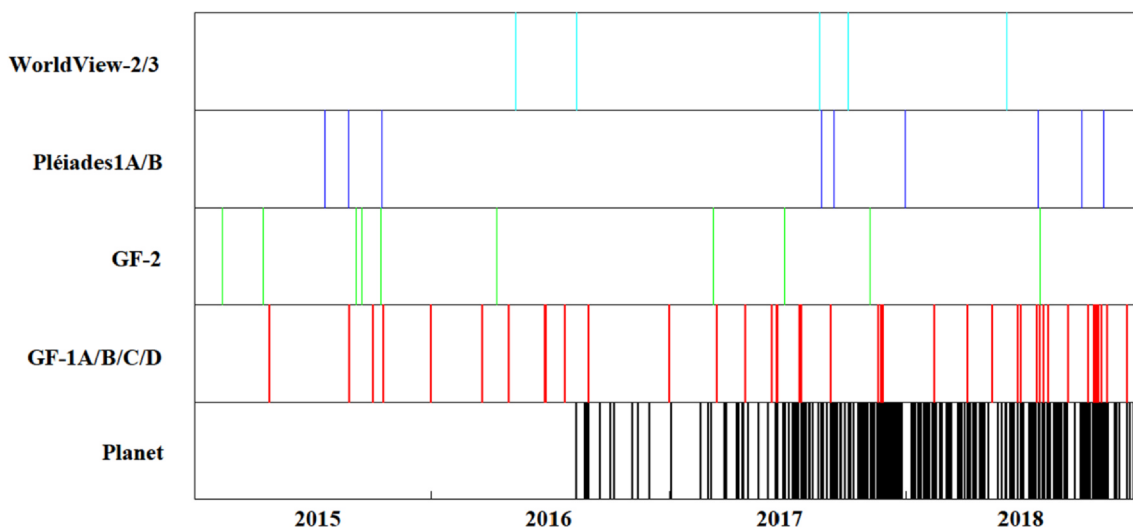


**Fig. 15.** The availability of WorldView-2/3 (0.5 m), Pléiades-1A/B (0.5 m), GF-2 (0.8 m), GF-1A/B/C/D PMS (2 m) and Planet images (3 m) for the crop season over the Xinghua tile from 2015 to 2018.

2010; Zhang et al., 2013; Jia et al., 2014), but it is rare for delineation of crop field boundaries. With either WorldView or Planet imagery alone, the classification accuracy of crop and non-crop objects was only 80% to 85%. The drawback with a single image source lay in the deficiency in crop field identification or boundary identification. By integrating the WorldView and Planet imagery, we were able to improve the recognition accuracy of crop and non-crop objects by up to 17% (Table 4). This represents a first attempt to combine a single VHR image with bi-temporal HR images for delineating the boundaries of crop fields.

Although the majority of field sizes were < 2.56 ha in this study (Fig. 16), the application of DESTIN should not be constrained to the regions characterized by small crop fields. We focused on small and very small crop fields because previous studies suggested that the automatic boundary delineation of small fields is more challenging (Persello et al., 2019). The new method should also be applicable to larger crop fields with the appropriate input WorldView and Planet imagery, if their coverage efficiency and cost is acceptable for the application. This speculation is supported by the finding that the best performance was seen on the large fields for both sites (Fig. 13). Compared to small fields, larger fields always exhibited lower  $S^{over}$ ,  $S_{under}$  and  $SEI$  values. The delineation for larger fields was more accurate since their boundaries were more prominent and easier to be detected with delineation algorithms (Persello et al., 2019). Since the development of DESTIN was based on VHR and HR imagery, future applications might be prioritized for delineating small and even very small crop fields given their spatial coverage capability and purchasing cost. Future research may be directed to evaluate the performance of

DESTIN for medium resolution imagery (e.g., Sentinel-2) or HR imagery from different sources (e.g., GF-1 & GF-2).

Traditionally, time series imagery and extensive prior knowledge about fields are the prerequisite for delineation of crop field boundaries (Yan and Roy, 2014, 2016; North et al., 2019). However, DESTIN only needs two HR images at critical points ( $NDVI_{Local-min}$  and  $NDVI_{Global-min}$ ) of the crop calendar paired with one VHR image in the peak season as the input data. These images could be collected from sophisticated satellite and airborne instruments, or from the emerging unmanned aerial systems (Zhang and Kovacs, 2012). In addition, DESTIN does not need prior knowledge about crop type distribution and training data for supervised classification. The operation of commonly used morphological post-processing was adopted in the DESTIN method for refining the crop field boundaries but this procedure could not be directly applied to the final output from the ENVI FX method, which resulted in numerous small noisy objects (Fig. 12c, d, g, &h).

Although we used Planet time series imagery to identify the temporal features, the thresholding for crop field recognition involved only a pair of Planet NDVI images. While using the knowledge-based temporal features for a new study are with similar major crops, the input for DESTIN would not need the expensive times series data. With the advantages of DESTIN mentioned above, it is extremely favorable to the automatic delineation of small crop field boundaries at county level or even larger scales in the future. This is particularly useful for developing countries that have the majority of small crop fields in the world (Lesiv et al., 2018). Although the crop field boundaries have been delineated accurately for the four subsets, under-segmentation could be seen at the fields with low magnitude of edge intensity. Future research

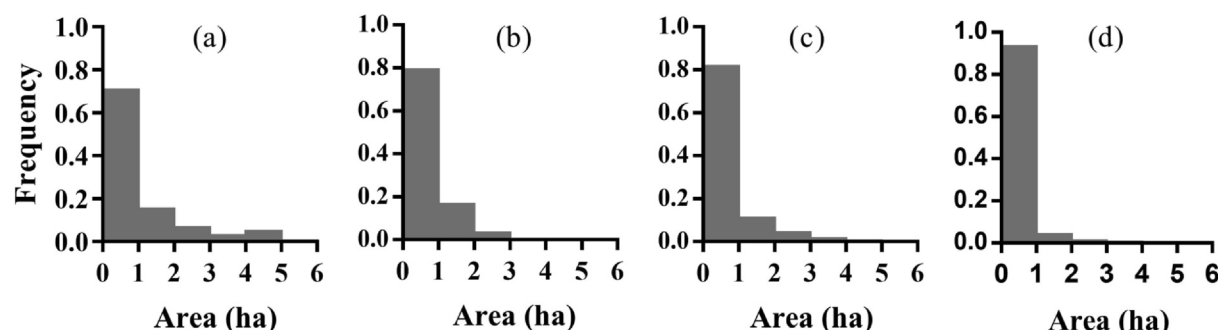


**Fig. 16.** Frequency distribution of sizes for the fields delineated over the subsets (a) HA1, (b) HA2, (c) XH1, and (d) XH2 with the DESTIN method. The two largest fields in HA1 (15.54 ha and 10.40 ha) were excluded from the frequency graph in (a) to keep the same area range for all plots.

should be directed to enhance the delineation at narrow edges.

The DESTIN method was based on the NDVI images merely and did not use the red edge (RE) band that is useful for distinguishing vegetation from non-vegetation (Miller et al., 1990; Segarra et al., 2020). The RE band was not included yet because it was unavailable in the Planet imagery. How to incorporate the RE band into the DESTIN procedures and whether it will make significant improvements still need to be further investigated. In addition, DESTIN was not yet applied to provincial or national level studies due to the high cost in acquiring cloud-free HR and VHR imagery over large areas. For large-scale applications to smallholder farming areas in developing countries, more work is needed to adjust DESTIN for the combination of HR and medium resolution images as replacement input data at a lower cost and higher chances of cloud-free coverage.

## 6. Conclusions

This study developed a new method for delineating the boundaries of crop fields with the integration of multi-sensor VHR and HR satellite imagery. The performance of crop field boundary delineation with DESTIN was evaluated with the reference polygons from ground surveys and further compared with the commonly used method ENVI FX. The results demonstrated that the integration of spatial and temporal information from WorldView and Planet imagery could remarkably improve the accuracy of crop field recognition, with the minimum improvement (12% in OA) for the XH1 subset and the maximum (17% in OA) for the HA1 subset over the use of WorldView or Planet imagery alone. These improvements by using DESTIN resulted from the spatial details for extracting objects and the temporal features of soil preparation and crop harvesting for distinguishing crop field objects from non-crop objects.

The majority of crop field boundaries were accurately delineated with both methods, but the boundaries with DESTIN appeared cleaner and closer to the reference than those with ENVI FX. Overall, DESTIN worked well for all these subsets and exhibited better performance. In contrast to ENVI FX, DESTIN was not prone to over-segmentation and yielded a better match with the reference boundaries. In addition, the delineation of crop field boundaries with DESTIN is straightforward without the need of sophisticated time series imagery and subjective parameterization for segmentation. The DESTIN method has great potential for delineation of crop field boundaries in smallholder farming systems, especially in the developing countries with fragmented distribution of crop fields.

## CRediT authorship contribution statement

**Tao Cheng:** Conceptualization, Methodology, Formal analysis, Investigation, Writing - review & editing. **Xusheng Ji:** Methodology, Software, Formal analysis, Investigation, Writing - original draft. **Gaoxiang Yang:** Methodology, Formal analysis, Writing - original draft. **Hengbiao Zheng:** Validation, Resources. **Jifeng Ma:** Validation, Resources. **Xia Yao:** Resources, Supervision. **Yan Zhu:** Funding acquisition, Project administration, Supervision. **Weixing Cao:** Conceptualization, Funding acquisition, Project administration, Resources, Supervision.

## Declaration of Competing Interest

The authors declare that they have no known competing financial interests or personal relationships that could have appeared to influence the work reported in this paper.

## Acknowledgment

This work was supported by the National Key R&D Program of

China (2016YFD0300601), the National Natural Science Foundation of China (41871259, 31725020), Jiangsu Collaborative Innovation Center for Modern Crop Production, China Postdoctoral Science Foundation (2019M651854), the Natural Science Fund of Jiangsu Province (SBK2019044119), the Academic Program Development of Jiangsu Higher Education Institutions (PAPD), and the Qinghai Project of Transformation of Scientific and Technological Achievements (2018-NK-126). We are grateful to the anonymous reviewers who provided helpful comments to improve the manuscript.

## Appendix A. Supplementary material

Supplementary data to this article can be found online at <https://doi.org/10.1016/j.compag.2020.105787>.

## References

- A, D., Zhao, W., Qu, X., Jing, R., Xiong, K., 2016. Spatio-temporal variation of vegetation coverage and its response to climate change in North China plain in the last 33 years. *Int. J. Appl. Earth Observat. Geoinform.*, 53, 103–117.
- Abdul, H.K., Raju, P.V., 2009. Use of high-resolution satellite data for the structural and agricultural inventory of tank irrigation systems. *Int. J. Remote Sens.* 30 (14), 3613–3623.
- Aksoy, S., Yalniz, I.Z., Tasdemir, K., 2012. Automatic detection and segmentation of orchards using very high resolution imagery. *IEEE Trans. Geosci. Remote Sens.* 50, 3117–3131.
- Alemu, M.M., 2016. Automated farm field delineation and crop row detection from satellite images. [online]. Available from: University of Twente.
- Ata-Ul-Karim, S.T., Yao, X., Liu, X., Cao, W., Zhu, Y., 2013. Development of critical nitrogen dilution curve of Japonica rice in Yangtze River Reaches. *Field Crops Res.* 149, 149–158.
- Baatz, M., Schape, A., 2000. Multiresolution segmentation: An optimization approach for high quality multiscale image segmentation. *Angew. Geographische Informat. verarbeitung* 12, 12–23.
- Basnyat, P., McConkey, B., Meinert, B., Gatkze, C., Noble, G., 2004. Agriculture field characterization using aerial photograph and satellite imagery. *IEEE Geosci. Remote Sens. Lett.* 1, 7–10.
- Bhalerao, A., Wilson, R., 1990. multiresolution image segmentation combining region and boundary information. In: Theory and Applications of Image Analysis: Selected Papers from the Seventh Scandinavian Conference. World Scientific, Singapore, pp. 148–161.
- Bleau, A., Leon, L.J., 2000. Watershed-based segmentation and region merging. *Comput. Vis. Image Underst.* 77, 317–370.
- Brown, L., 1995. Who Will Feed China? Wake up Call for a Small Planet. Norton and Company., New York, NY, USA.
- Butenuth, M., Straub, B., Heipke, C., 2004. Automatic extraction of field boundaries from aerial imagery. In: KDNet Symposium on Knowledge-Based Services for the Public Sector, pp. 14–25.
- Canny, J., 1986. Computational approach to edge detection. *IEEE Trans. Pattern Anal. Mach. Intell.* 8, 679–698.
- Chen, B., Qiu, F., Wu, B., Du, H., 2015. Image segmentation based on constrained spectral variance difference and edge penalty. *Remote Sensing* 7, 5980–6004.
- Conrad, C., Fritsch, S., Zeidler, J., Rücker, G., Dech, S., 2010. Per-field irrigated crop classification in arid central Asia using SPOT and ASTER data. *Remote Sensing* 2, 1035–1056.
- Debats, S.R., Luo, D., Estes, L.D., Fuchs, T.J., Taylor, K.K., 2016. A generalized computer vision approach to mapping crop fields in heterogeneous agricultural landscapes. *Remote Sens. Environ.* 179, 210–221.
- Dong, J., Xiao, X., Menarguez, M.A., Zhang, G., Qin, Y., Thau, D., Biradar, C., Moore 3rd, B., 2016. Mapping paddy rice planting area in northeastern Asia with Landsat 8 images, phenology-based algorithm and Google Earth Engine. *Remote Sens. Environ.* 185, 142–154.
- FAO, 2009. How to feed the world in 2050, Rome.
- Fetai, B., Ošir, K., Kosmatin Fras, M., Liseč, A., 2019. Extraction of visible boundaries for cadastral mapping based on UAV imagery. *Remote Sensing* 11, 1510.
- Fritz, S., See, L., McCallum, I., You, L., Bun, A., Molchanova, E., Duerauer, M., Albrecht, F., Schill, C., Perger, C., Havlik, P., Mosnier, A., Thornton, P., Wood-Sichra, U., Herrero, M., Becker-Reshef, I., Justice, C., Hansen, M., Gong, P., Abdel Aziz, S., Cipriani, A., Cumani, R., Cecchi, G., Conchedda, G., Ferreira, S., Gomez, A., Haffani, M., Kayitakire, F., Malanding, J., Mueller, R., Newby, T., Nonguierma, A., Olusegun, A., Ortner, S., Rajak, D.R., Rocha, J., Schepaschenko, D., Schepaschenko, M., Terekhov, A., Tiangwa, A., Vancutsem, C., Vintrou, E., Wenbin, W., van der Velde, M., Dunwoody, A., Kraxner, F., Obersteiner, M., 2015. Mapping global cropland and field size. *Glob. Change Biol.* 21 (5), 1980–1992.
- Gonzalez, R.C., Woods, R.E., 2008. Digital Image Processing, 3rd ed. Pearson Prentice Hall, Upper Saddle River, NJ.
- Graesser, J., Ramankutty, N., 2017. Detection of cropland field parcels from Landsat imagery. *Remote Sens. Environ.* 201, 165–180.
- Geerten, R., 2009. An algorithm to classify and monitor seasonal variations in vegetation phenologies and their inter-annual change. *ISPRS J. Photogramm. Remote Sens.* 64

- (4), 422–431.
- Houborg, R., McCabe, M., 2016. High-resolution NDVI from Planet's constellation of Earth observing nano-satellites: A new data source for precision agriculture. *Remote Sensing* 8, 768.
- Hossain, M.D., Chen, D., 2019. Segmentation for Object-Based Image Analysis (OBIA): A review of algorithms and challenges from remote sensing perspective. *ISPRS J. Photogramm. Remote Sens.* 150, 115–134.
- Helmholz, P., Rottensteiner, F., Heipke, C., 2014. Semi-automatic verification of cropland and grassland using very high resolution mono-temporal satellite images. *ISPRS J. Photogramm. Remote Sens.* 97, 204–218.
- ITT Visual Information Solutions, 2008. ENVI Feature Extraction User's Guide. Harris Geospatial Solutions, Broomfield, CO, USA.
- Jia, K., Liang, S., Zhang, N., Wei, X., Gu, X., Zhao, X., Yao, Y., Xie, X., 2014. Land cover classification of finer resolution remote sensing data integrating temporal features from time series coarser resolution data. *ISPRS J. Photogramm. Remote Sens.* 93, 49–55.
- Jin, X., 2012. Segmentation-based image processing system. U.S. Patent 8,260,048, filed Nov. 14, 2007, and issued Sept. 4, 2012.
- Ji, Y., 1996. Delineating agricultural field boundaries from TM imagery using dyadic wavelet transforms. *ISPRS J. Photogramm. Remote Sens.* 51 (6), 268–283.
- Lemaire, G., Jeuffroy, M.-H., Gastal, F., 2008. Diagnosis tool for plant and crop N status in vegetative stage. *Eur. J. Agron.* 28, 614–624.
- Li, D., Zhang, G., Wu, Z., Yi, L., 2010. An edge embedded marker-based watershed algorithm for high spatial resolution remote sensing image segmentation. *IEEE Trans. Image Process.* 19, 2781–2787.
- Li, P., Guo, J., Song, B., Xiao, X., 2011. A multilevel hierarchical image segmentation method for urban impervious surface mapping using very high resolution imagery. *IEEE J. Sel. Top. Appl. Earth Obs. Remote Sens.* 4 (1), 103–116.
- Li, W., Jiang, J., Guo, T., Zhou, M., Tang, Y., Wang, Y., Zhang, Y., Cheng, T., Zhu, Y., Cao, W., Yao, X., 2019. Generating red-edge images at 3 m spatial resolution by fusing Sentinel-2 and Planet satellite products. *Remote Sensing* 11, 1422.
- Lesiv, M., Laso Bayas, J.C., See, L., Duerauer, M., Dahlia, D., Durando, N., Hazarika, R., Kumar Sahariah, P., Vakolyuk, M., Blyshchyk, V., Bilous, A., Perez-Hoyos, A., Gengler, S., Prestele, R., Bilous, S., Akhtar, I.U.H., Singha, K., Choudhury, S.B., Chetri, T., Malek, Ž., Bungnamei, K., Saikia, A., Sahariah, D., Narzary, W., Danylo, O., Sturn, T., Karner, M., McCallum, I., Schepaschenko, D., Molchanova, E., Fraisl, D., Moorthy, I., Fritz, S., 2018. Estimating the global distribution of field size using crowdsourcing. *Glob. Change Biol.* 25 (1), 174–186.
- Ministry of Natural Resources of the People's Republic of China, 2017. [http://gi.mnr.gov.cn/201805/20180518\\_1776792.html](http://gi.mnr.gov.cn/201805/20180518_1776792.html).
- Miller, J.R., Hare, E.W., Wu, J., 1990. Quantitative characterization of the vegetation red edge reflectance 1. An inverted-Gaussian reflectance model. *Int. J. Remote Sens.* 11, 1755–1773.
- Moigne, J.L., Tilton, J.C., 2002. Refining image segmentation by integration of edge and region data. *IEEE Trans. Geosci. Remote Sens.* 33, 605–615.
- Mostafa, Yasser, 2020. A new shape descriptor for road network separation from parking lots and intersection detection on VHR remote sensing images. *Int. J. Remote Sens.* 41, 4226–4237.
- Musat, G., Colezea, M., Pop, F., Negru, C., Mocanu, M., Esposito, C., Castiglione, A., 2018. Advanced services for efficient management of smart farms. *J. Parallel Distrib. Comput.* 116, 3–17.
- Mueller, M., Segl, K., Kaufmann, H., 2004. Edge- and region-based segmentation technique for the extraction of large, man-made objects in high-resolution satellite imagery. *Pattern Recogn.* 37, 1619–1628.
- Neigh, C., Carroll, M., Wooten, M., McCarty, J., Powell, B., Husak, G., Enenkel, M., Hain, C., 2018. Smallholder crop area mapped with wall-to-wall WorldView sub-meter panchromatic image texture: A test case for Tigray, Ethiopia. *Remote Sens. Environ.* 212, 8–20.
- North, H.C., Pairman, D., Belliss, S.E., 2019. Boundary delineation of agricultural fields in multitemporal satellite imagery. *IEEE J. Sel. Top. Appl. Earth Obs. Remote Sens.* 12, 237–251.
- Persello, C., Tolpekin, V.A., Bergado, J.R., de By, R.A., 2019. Delineation of agricultural fields in smallholder farms from satellite images using fully convolutional networks and combinatorial grouping. *Remote Sens. Environ.* 231, 111253.
- Poursanidis, D., Chrysoulakis, N., Mitraka, Z., 2015. Landsat 8 vs. Landsat 5: A comparison based on urban and peri-urban land cover mapping. *Int. J. Appl. Earth Obs. Geoinf.* 35, 259–269.
- Peña-Barragán, J.M., Ngugi, M.K., Plant, R.E., Six, J., 2011. Object-based crop identification using multiple vegetation indices, textural features and crop phenology. *Remote Sens. Environ.* 115, 1301–1316.
- Qin, Y., Xiao, X., Dong, J., Zhou, Y., Zhu, Z., Zheng, G., Du, G., Jin, C., Kou, W., Wang, J., Li, X., 2015. Mapping paddy rice planting area in cold temperature climate region through analysis of time series Landsat 8 (OLI), Landsat 7 (ETM+) and MODIS imagery. *Remote Sens. Environ.* 105, 220–233.
- Rydberg, A., Borgefors, G., 2001. Integrated method for boundary delineation of agricultural fields in multispectral satellite images. *IEEE Trans. Geosci. Remote Sens.* 39 (11), 2514–2520.
- Rishikeshan, C.A., Ramesh, H., 2018. An automated mathematical morphology driven algorithm for water body extraction from remotely sensed images. *ISPRS J. Photogramm. Remote Sens.* 146, 11–21.
- Turker, M., Kok, H.E., 2013. Field-based sub-boundaries extraction from remote sensing imagery using perceptual grouping. *ISPRS J. Photogramm. Remote Sens.* 79, 106–121.
- Sadeh, Y., Zhu, X., Chen, K., Dunkerley, D., 2019. Sowing date detection at the field scale using CubeSats remote sensing. *Comput. Electron. Agric.* 157, 568–580.
- Segarra, J., Buchaillot, M.L., Araus, J.L., Kefauver, S.C., 2020. Remote sensing for precision agriculture: Sentinel-2 improved features and applications. *Agronomy* 10, 641.
- Shrivakshan, G.T., Chandrasekar, C., 2012. A comparison of various edge detection techniques used in image processing. *Int. J. Comput. Sci. Issues* 9, 269–276.
- Sun, R., Chen, S., Su, H., Mi, C., Jin, N., 2019. The effect of NDVI time series density derived from spatiotemporal fusion of multisource remote sensing data on crop classification accuracy. *ISPRS Int. J. Geo-Inf.* 8, 502.
- Tilman, D., Fargione, J., Wolff, B., D'Antonio, C., Dobson, A., Howarth, R., Schindler, D., Schlesinger, W.H., Simberloff, D., Swackhamer, D., 2001. Forecasting agriculturally driven global environmental change. *Science* 292, 281–284.
- Wang, J., Song, J., Chen, M., Yang, Z., 2015. Road network extraction: a neural-dynamic framework based on deep learning and a finite state machine. *Int. J. Remote Sens.* 36, 3144–3169.
- Watkins, B., Niekerk, A., 2019. A comparison of object-based image analysis approaches for field boundaries delineation using multi-temporal Sentinel-2 imagery. *Comput. Electron. Agric.* 158, 294–302.
- Waldner, F., Canto, G., Defourny, P., 2015. Automated annual cropland mapping using knowledge-based temporal features. *ISPRS J. Photogramm. Remote Sens.* 110, 1–13.
- Weisseiner, C.J., García-Feced, C., Paracchini, M.L., 2015. A new view on EU agricultural landscapes: Quantifying patchiness to assess farmland heterogeneity. *Ecol. Ind.* 61, 317–327.
- Wuest, B., Zhang, Y., 2009. Region based segmentation of QuickBird multispectral imagery through band ratios and fuzzy comparison. *ISPRS J. Photogramm. Remote Sens.* 64, 55–64.
- Xiao, X.M., Boles, S., Liu, J.Y., Zhuang, D.F., Frolking, S., Li, C.S., Salas, W., Moore, B., 2005. Mapping paddy rice agriculture in southern China using multi-temporal MODIS images. *Remote Sens. Environ.* 95, 480–492.
- Xiong, J., Thenkabail, P.S., Gumma, M.K., Teluguntla, P., Poehnelt, J., Congalton, R.G., Yadav, K., Thau, D., 2017. Automated cropland mapping of continental Africa using Google Earth Engine cloud computing. *ISPRS J. Photogramm. Remote Sens.* 126, 225–244.
- Yan, L., Roy, D.P., 2014. Automated crop field extraction from multi-temporal Web Enabled Landsat Data. *Remote Sens. Environ.* 144, 42–64.
- Yan, L., Roy, D.P., 2016. Conterminous United States crop field size quantification from multi-temporal Landsat data. *Remote Sens. Environ.* 172, 67–86.
- Yang, J., He, Y., Caspersen, J., Jones, T., 2015. A discrepancy measure for segmentation evaluation from the perspective of object recognition. *ISPRS J. Photogramm. Remote Sens.* 101, 186–192.
- Yang, Y., Huang, Q., Wu, W., Luo, J., Gao, L., Dong, W., Wu, T., Hu, X., 2017. Geo-parcel based crop identification by integrating high spatial-temporal resolution imagery from multi-source satellite data. *Remote Sensing* 9, 1298–1317.
- Yu, Q., Shi, Y., Tang, H., Yang, P., Xie, A., Liu, B., Wu, W., 2017. eFarm: A tool for better observing agricultural land systems. *Sensors* 17, 453.
- Zhang, Y., 1996. A survey on evaluation methods for image segmentation. *Pattern Recogn.* 29, 1335–1346.
- Zhang, C., Kovacs, J.M., 2012. The application of small unmanned aerial systems for precision agriculture: A review. *Precis. Agric.* 13, 693–712.
- Zhang, H., Fritts, J.E., Goldman, S.A., 2008. Image segmentation evaluation: a survey of unsupervised methods. *Comput. Vis. Image Underst.* 110, 260–280.
- Zhang, W., Li, A., Jin, H., Bian, J., Zhang, Z., Lei, G., Qin, Z., Huang, C., 2013. An enhanced spatial and temporal data fusion model for fusing Landsat and MODIS surface reflectance to generate high temporal Landsat-like data. *Remote Sensing* 5, 5346–5368.
- Zhang, X., Feng, X., Xiao, P., He, G., Zhu, L., 2015. Segmentation quality evaluation using region-based precision and recall measures for remote sensing images. *ISPRS J. Photogramm. Remote Sens.* 102, 73–84.
- Zhong, L., Hu, L., Yu, L., Gong, P., Biging, G.S., 2016. Automated mapping of soybean and corn using phenology. *ISPRS J. Photogramm. Remote Sens.* 119, 151–164.
- Zhong, Li, Gong, P., Biging, G., 2014. Efficient corn and soybean mapping with temporal extendability: A multi-year experiment using Landsat imagery. *Remote Sens. Environ.* 140, 1–13.
- Zhu, X., Chen, J., Gao, F., Chen, X., Masek, J.G., 2010. An enhanced spatial and temporal adaptive reflectance fusion model for complex heterogeneous regions. *Remote Sens. Environ.* 114, 2610–2623.